https://doi.org/10.5194/egusphere-2026-3764
Preprint. Discussion started: 7 July 2026

Evolution of deep-water circulation in the North-East Atlantic during the latest Miocene warming

Boris-Theofanis Karatsolis[1,2], Matthias Sinnesael[3], Tom Dunkley Jones[4], Anna Joy Drury[5], Leah LeVay[6], Anne Briais[7], Ross Parnell-Turner[8], Emma Hanson[4], Paul N. Pearson[9], Margaret Morris[8], Haley Svadlenak[8], Sidney R. Hemming[10,11], Claire E. Jasper[12,10,11], Anita Di Chiara[13], Sara Satolli[14], Sarah Friedman[15,16], Deepa Dwyer[17], Philippe Claeys[1,18]

[1]Archaeology, Environmental changes & Geo-Chemistry, Vrije Universiteit Brussel, Pleinlaan 2, 1050 Brussels, Belgium.
[2]Department of Geosciences, University of Fribourg, Chemin du Musée 6, 1700 Fribourg, Switzerland
[3]Geology, School of Natural Sciences, Trinity College Dublin, The University of Dublin, College Green, Dublin 02, Ireland.
[4]School of Geography, Earth and Environmental Sciences, University of Birmingham, Birmingham B15 2TT, United Kingdom.
[5]School of Geography, Geology and the Environment, University of Leicester, Leicester LE1 7RH, UK.
[6]Scientific Ocean Drilling, Texas A&M University, 1000 Discovery Drive, College Station TX 77845, USA.
[7]Geo-Ocean, Centre National de la Recherche Scientifique (CNRS), Institut Universitaire Européen de la Mer, Rue Dumont d'Urville, 29280 Plouzané, France.
[8]Institute of Geophysics & Planetary Physics, Scripps Institution of Oceanography, University of California, San Diego, La Jolla CA 92093, USA.
[9]Department of Earth Sciences, University College London, Gower Street, London WC1E 6BT, United Kingdom.
[10]Department of Earth and Environmental Sciences, Columbia University, New York, NY, USA
[11]Lamont-Doherty Earth Observatory, Columbia University, Palisades, NY, USA
[12]Ocean Sciences Department, University of California, Santa Cruz, Santa Cruz, CA, USA
[13]Istituto Nazionale di Geofisica e Vulcanologia, Via di Vigna Murata 605, 00143 Roma, Italy.
[14]Department of Engineering and Geology, University of Chieti-Pescara, Viale Pindaro 42, 65127 Pescara, Italy.
[15]School of Earth, Environment & Sustainability, Georgia Southern University, Statesboro, GA 30458, USA.
[16]Department of Geological Sciences, New Mexico State University, Las Cruces, NM 88003, USA.
[17]College of Earth Ocean and Atmospheric Sciences, Oregon State University, 1500 SW, Jefferson Way, Corvallis OR 97331, USA.
[18]Pacific Centre for Isotope and Geochemical Research, Dept Earth, Ocean and Atmospheric Sciences, University of British Columbia, Vancouver, BC, Canada

Correspondence to: Boris Theofanis Karatsolis (boris.karatsolis@unifr.ch)

Abstract. Understanding the possible responses of Atlantic Meridional Overturning Circulation (AMOC) to climate warming is one of the major challenges of modern oceanography. Today, the lower (deeper) southward flowing limb of AMOC consists of the North Atlantic deep water (NADW), which is predominantly formed by deepwater convection in the ocean basins to the north and south of Iceland. The southward transit of deep water formed in the northerly basins (Greenland-Iceland-Norwegian Seas) is constrained by gateway geometry to two major flow pathways to the east and west of Iceland. To the south of Iceland extensive deep-sea sediment archives, in the form of contourite drifts, are deposited by these currents and have provided critical information about AMOC and NADW dynamics through the Pleistocene. Here we make use of recently recovered cores from one of these sediment drifts (Gardar Drift, IODP Expedition 395, Site U1564,), that records the deep Iceland-Scotland Overflow water (ISOW) dynamics back to the warm climates states of the late Miocene to Pliocene. By combining

https://doi.org/10.5194/egusphere-2026-3764
Preprint. Discussion started: 7 July 2026

sedimentological and X-Ray fluorescence derived elemental proxy evidence, we reconstructed deep ocean current activity and carbonate preservation between 5.0-6.2 million years ago (Ma). The record supports the periodic presence of deep currents since the latest Miocene, as well as a distinct ISOW weakening that coincided with the global warming trend, and the severe restriction on Mediterranean Outflow Water, just before the Miocene-Pliocene boundary. Low carbonate preservation hints to the presence of corrosive water masses in the North Atlantic following the termination of the Messinian salinity crisis.

1 Introduction

Marine sediments recovered by scientific ocean drilling into the seafloor provide among the most continuous records of past climatic fluctuations on the hundreds- to millions of years timescales. The physical and geochemical properties of lithogenic grains and microfossils can be used as proxies that reflect changes in surface and deep-ocean temperature, phytoplankton productivity, and ocean circulation dynamics. In recent decades, researchers have increasingly focused on past warm periods to gather highly resolved evidence on the response of the marine system to increasing temperatures and CO_2 levels (e.g., Burke et al., 2018; Foster et al., 2018; Loutre and Berger, 2003). The Pliocene (~5.33–2.58) represents a key period that demonstrates similar-to-today CO_2 levels and significantly warmer than present ocean surface temperatures (e.g., Steinthorsdottir et al., 2021; Tierney et al., 2020; Herbert et al., 2016; Fedorov et al., 2013; Ravelo et al., 2004). This overall warm period was preceded by global cooling and aridification in the Miocene (hereafter referred to as LMC: late Miocene Cooling; Fig. 1), which lasted between 7.2–5.5 Ma and was terminated by an abrupt shift to a warming trend close to the Miocene–Pliocene boundary (e.g., Holbourn et al., 2018; Herbert et al., 2016; Fig. 1). This late Miocene Warming (LMW; Fig. 1) led to major climatic reorganizations, including a transition to a wetter climate in the Southern Hemisphere (Sniderman et al., 2016; deAzevedo et al., 2023), as well as stronger Asian summer monsoon but drier conditions in Central Asia (Ao et al., 2021). In the marine realm, high-latitude sea surface temperatures (SST) increased by up to 5 °C (e.g., compilation by Herbert et al. 2016; Fig. 1). While attention has been given to the more recent mid-Pliocene warm period (~3.3–3 Ma, e.g., Tindall & Haywood 2020; Haywood et al., 2016; Raymo et al., 1996), the drivers and impact of the latest Miocene-early Pliocene warming on major marine systems remain poorly constrained, partially due to fewer high-resolution records being available for this period. In this study, we provide new insights on North Atlantic ocean circulation through this climatic transition from the Miocene to the Pliocene (5.0-6.2 Ma) using sediments cored during International Ocean Discovery Program (IODP) Expedition 395 (Fig. 2).

https://doi.org/10.5194/egusphere-2026-3764
Preprint. Discussion started: 7 July 2026

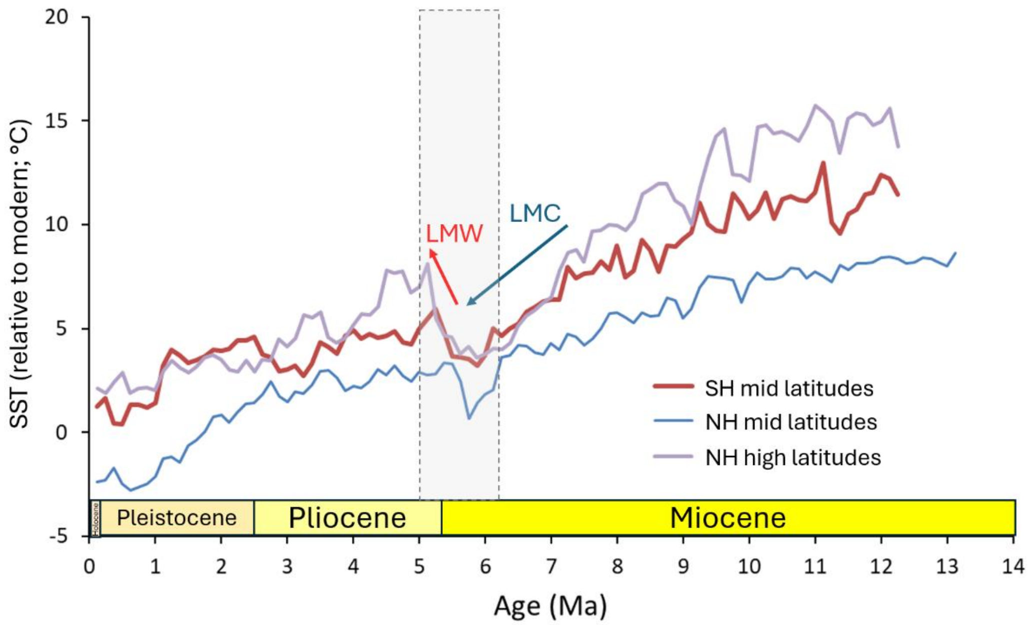

Figure 1: Alkenone derived sea surface temperature (SST; in °C) relative to modern for the last 14 Ma. The records for the Northern Hemisphere (NH) mid- (blue line) and high latitudes (purple line), and Southern Hemisphere (SH) mid-latitudes (red line) are shown, as compiled by Herbert et al., 2016. The late Miocene cooling (LMC) trend is followed by the global increase in SSTs that occurred close to the Miocene-Pliocene transition. The shaded area shows the interval investigated in this study. Blue arrow indicates the late Miocene cooling and red arrow the late Miocene warming.

Among the systems that can shed light to paleoclimatic conditions during past warm intervals, the formation of deep-water masses and the circulation of bottom ocean currents are important for regulating the CO_2 solubility pump (Volk and Hoffert 1985). In this regard, the North Atlantic is a crucial region, acting as a major CO_2 sink (Takahashi et al., 2009), an intersection for important ocean circulation components (Olafsson et al., 2020), and an area of high primary production (Uitz et al., 2010; Fig. 2). In the modern ocean, the North Atlantic current (NAC) moves saline surface water from tropical regions towards the north, which subsequently cools in the Nordic and Labrador seas, sinks, and forms what is known as the North Atlantic deep water (NADW; Fig. 2). The NADW powers strong south-flowing bottom currents and constitutes the lower limb of what is known as the Atlantic Meridional Overturning Circulation (AMOC) and the global "conveyor belt" (Richardson, 2008). Two of the main components that combine to produce NADW are the Denmark Strait overflow water (DSOW), and the Iceland-Scotland overflow water (ISOW), which respectively, flow southwards through straits to the west and east of Iceland (Fig. 2). Since deep-water formation is a key mechanism for removing CO_2 from the surface of the ocean, any weakening of this system could reduce the efficiency of carbon uptake and storage, (e.g., Steinfeldt et al., 2009), possibly acting as positive feedback to warming. In addition, there is strong evidence suggesting that such a slowdown can be a response to rising CO_2 levels and increasing ocean stratification in the North Atlantic (Wang et al., 2014; Stocker and Schmittner, 1997). Understanding the evolution and activity of these deep-water masses during past warm intervals can therefore provide insights into the role of the global conveyor belt in warm climate states, and its role in climate feedback mechanisms.

https://doi.org/10.5194/egusphere-2026-3764
Preprint. Discussion started: 7 July 2026

The sparsity of studies investigating North Atlantic deep-water formation and circulation across the latest Miocene warming is due to the poor availability of contourite drift records from before the Late Pliocene (e.g., Parnell-Turner et al., 2025; 2015). These rapidly accumulating sedimentary drift sequences can record deep-water formation and associated bottom current activity, with sufficient sedimentation rates to generate high-resolution paleoceanographic timeseries (e.g., Rebesco et al., 2014; Wold, 1994). Drilling through these thick drift deposits is particularly challenging, especially close to the deep-water source areas and pathways, where sedimentation rates are very high. Therefore, most previous reconstructions of early-Pliocene conveyor belt dynamics, NADW formation and North Atlantic paleoclimate focused on lower latitude sites (e.g., Karas et al., 2017; Bell et al., 2015; Billups et al., 1998; Haug and Tiedemann, 1998) or relied on seismic profile interpretation and synthesis to infer drift deposition (e.g., Müller-Michaelis et al., 2013, 2014). One of the few high-latitude North Atlantic sites to recover this interval and provide high-resolution proxy data, Ocean Drilling Program (ODP) Site 982 on the Rockall Plateau (Hodell et al., 2001; Drury et al., 2018, and references therein), records the stepwise transition to a warmer state near the onset of the Pliocene (Herbert et al., 2016). However, it is located on a bathymetric high (~1100 m below sea level) and is therefore a much less sensitive recorder of intermediate-to-deep bottom current activity.

Sediment core availability in this critical region significantly improved in the summers of 2021 and 2023 when IODP Expeditions 395C and 395 successfully drilled a series of sites located across a North-Atlantic high-latitude transect (~60°N; Parnell-Turner et al., 2025). The base of two of the main North Atlantic drift deposits (Björn, Gardar) was recovered at three sites, which all contain sedimentary records spanning the late Miocene–Pliocene. Site U1564 on the Garder Drift (Fig. 2) appears to have continuous sedimentation since the late Miocene (Parnell-Turner et al., 2025; Sinnesael et al., 2025) and was therefore our chosen location to apply a series of proxy reconstructions. Specifically, we present new records of lithological changes, sedimentation rate estimates, as well as X-ray fluorescence (XRF)-derived elemental ratios. A newly constructed astrochronology informed by a bio-magneto chronostratigraphic framework enables comparison of IODP Site U1564 with ODP Site 982, where pelagic $CaCO_3$ content fluxes, possibly linked to marine paleoproductivity, have been reported (e.g., Diester-Haass et al., 2005). This comparison allows for an integrated reconstruction of shallow-to-intermediate (ODP Site 982; ~1134m water depth) versus deeper water mass activity (Site U1564; ~2208m water depth) and $CaCO_3$ preservation in the area. The results are interpreted here within the context of sea surface and deep ocean temperature changes in the North Atlantic region as well as major tectonic events that occurred during this period, such as the Messinian Salinity Crisis (MSC: 5.96–5.3 Ma; Krijsgman et al., 1999) and the opening of the Bering Strait (5.5–4.8 Ma; Gladenkov et al., 2002, and references therein). Finally, we assess the stability of deep-water formation in these warmer climate states.

https://doi.org/10.5194/egusphere-2026-3764
Preprint. Discussion started: 7 July 2026

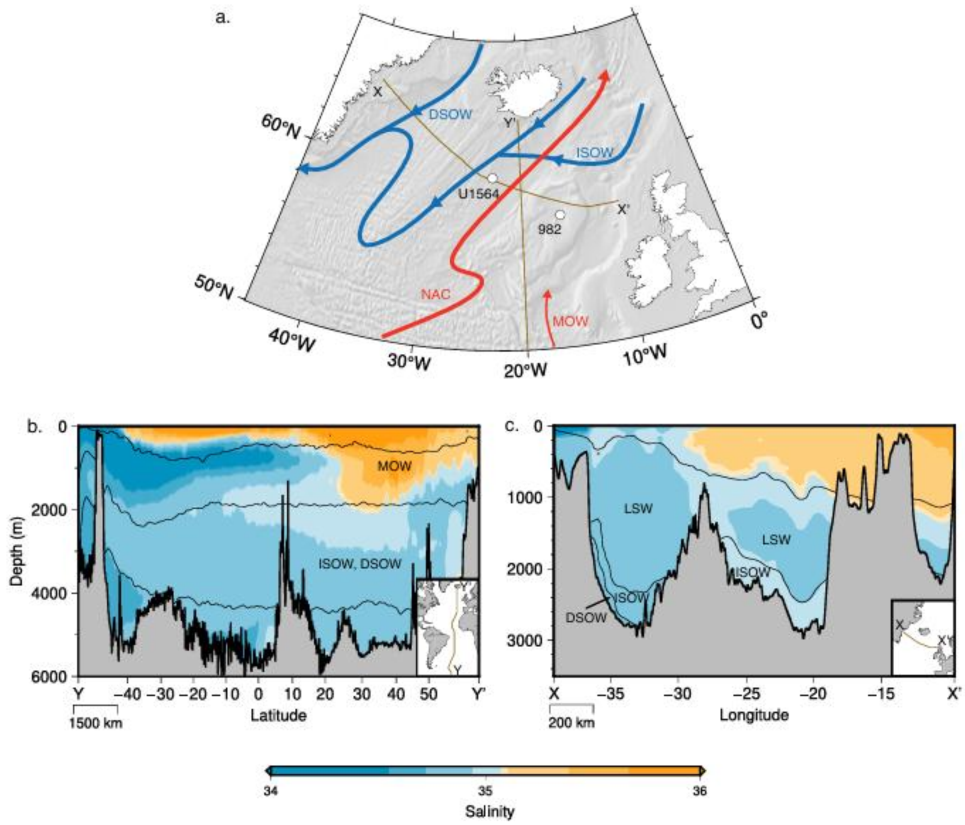

Figure 2: Atlantic Meridional Overturning Circulation pathway and main Atlantic Ocean water masses. a) North Atlantic Ocean map including main ocean circulation pathways and discussed drilling sites. White circles: Expedition 395 Site U1564 (Parnell-Turner et al., 2025) and ODP Leg 162 Site 982 (Jansen et al., 1996). DSOW = Denmark Strait Overflow Water; ISOW = Iceland–Scotland Overflow Water; LSW: Labrador Sea Water; NAC = North Atlantic Current; Salinity profiles for line b) Y-Y' and c) line X-X' showing the major water masses present in the North Atlantic today. Components of DSOW, ISOW and LSW meet south of Greenland and flow southwards as NADW. Neutral density contours are placed at 27.10, 27.90, and 28.10 kg m^{-3} for line Y-Y' and 27.10, 27.70, 28, and 28.15 kg m^{-3} for line X-X' (based on Liu & Tanhua, 2021). Profiles were made using GLODAPv2.2023 (Lauvset et al., 2023; 2022; Olsen et al., 2020; 2019; 2016; Key et al., 2015) and ETOPO1 Global Relief Model (NOAA National Geophysical Data Center. 2009: ETOPO1 1 Arc-Minute Global Relief Model. NOAA National Centers for Environmental Information. Accessed [December 3, 2025]; Amante et al., 2009)

https://doi.org/10.5194/egusphere-2026-3764
Preprint. Discussion started: 7 July 2026

2 Material and Methods

2.1 Study area, Site U1564

IODP Site U1564 (59°51.0366′N, 23°15.9858′W) is located in the NE Atlantic Ocean, east of the Reykjanes Ridge, within the Gardar Drift depositional system (Fig. 2; ~2208m). During Expeditions 395 and 395C, six holes were drilled at this site. The deepest drillhole, U1564F, reached the basaltic basement at ~997 m core depth below seafloor (method A; CSF-A), with basal sediments dating back to the earliest Oligocene, ~32 Ma (Parnell-Turner et al., 2025). A composite splice extending from present to the late Miocene (based on shipboard stratigraphy; Parnell-Turner et al., 2025) was generated by correlating the core magnetic susceptibility from three holes (U1564C, D, and E). This study focuses on core sections between ~650–549 m CCSF (core composite depth below seafloor), which correspond to the latest Miocene to earliest Pliocene (6.2-5.0 Ma). The investigated interval falls entirely within Lithological Unit II, which consists of alternating layers of nannofossil chalk with silty clay and silty claystone with nannofossils (Parnell-Turner et al., 2025). Under the modern ocean circulation regime, the area is influenced by the activity of the North Atlantic Current (NAC; Fig. 2) in the upper layers of the water column, and the ISOW-related currents at its deeper parts (e.g., Bianchi and McCave, 2000; Orvik and Niiler, 2002). More specifically, Site U1564 sits at the modern depth range of North Atlantic ISOW related deposition within the Gardar Drift system, as reported by Bianchi and McCave (2000).

2.2 X-ray fluorescence and $CaCO_3$ content

Elemental ratios are derived from X-ray fluorescence (XRF) elemental intensity measurements made on archive core-section halves at the IODP Gulf Coast Repository in College Station, Texas, USA. This non-destructive method uses the fluorescence emitted by elements, after an X-Ray beam with variable electrical potential (excitation voltage) hits the surface of the sediment. In this case, three energies (10, 30, and 50 keV) were measured using a 3rd generation Avaatech XRF scanner (XRF1). This instrument is equipped with a water-cooled, 100 W rhodium side-window x-ray tube and allows for the addition of various filters (detailed below). Measurements were made at discrete points close to the center line and within a preset grid of 5 cm steps. When necessary, adjustments were made to the grid based on the state of the sediment surface (disturbance, voids). The instrument set up included a tube current of 0.16 mA and no filters for the 10 keV measurements, a tube current of 1.25 mA and a Pd filter for the 30 keV measurements, and a tube current of 0.75 mA and a Cu filter for the 50 keV measurement. All sample rows with positive Argon values were removed, since such values are possible indicators of reduced contact between the XRF sensor and the surface of the sediment (air returns positive and high Argon values).

A suite of elements was counted, including Ca, K, Ti, Rb, and Zr, which are considered here. Specifically, we discuss the Ca/Ti, Zr/Rb and Ti/K ratios. In open marine settings, a ratio between the contents in Ca and an element linked to an eroded terrigenous component (Ti, Fe, Al) can be used as an indicator of the relative contribution of carbonate biogenic sediment (compared to lithogenic), sourced from calcifying organisms such as coccolithophores and foraminifera (e.g., Drury et al.,

https://doi.org/10.5194/egusphere-2026-3764
Preprint. Discussion started: 7 July 2026

2021). Here, we use the natural logarithm of the elemental ratio of Ca/Ti (measured at 10 keV), in combination with the low-resolution shipboard $CaCO_3$ (wt%) measurements (Parnell-Turner et al., 2025), to generate a high-resolution calibrated $CaCO_3$ content record (time steps of 500 years–1.500 kyrs). When the stratigraphic position of the samples with shipboard $CaCO_3$ (wt%) measurements did not correspond with the stratigraphic position of the XRF core scanning measurements, the corresponding elemental ratio was estimated by linear interpolation between the nearest XRF measurements, below and above the $CaCO_3$ measurement, respectively (interpolated ln (Ca/Ti); Fig. 3). The interval for this comparison was between ~491m CCSF and the end of the splice (~673 m CCSF), in order to include as many data points as possible (Fig. S1). Measurements above ~491m CCSF were not used, due to the significant change in depositional regime that occurred during the Late Pliocene at approximately this level (Sinnesael et al., 2025). The high-resolution calibrated $CaCO_3$ concentration record was derived from the XRF elemental ratios using the linear relationship shown in Figure 3. The approach of calibrating an XRF-derived biogenic/terrigenous elemental ratio towards a $CaCO_3$ concentration record has been previously applied to other sites, including South Atlantic ODP Site 1264 (e.g., Ca/Fe; Drury et al., 2021; Liebrand et al., 2016), and allows the detailed investigation of $CaCO_3$ dissolution and calcifying plankton-related paleoproductivity.

Two more elemental ratios, Zr/Rb and Ti/K, were used as proxies for bottom current strength and provenance, respectively. A higher Zr/Rb ratio can be used as an indicator of higher zircon content in coarser grained sediments deposited under stronger current regimes, based on previous interpretations established in current-sorted sediments such as drift and glaciomarine deposits (e.g., Wu et al., 2020; Lamy et al., 2015). A higher Ti/K ratio indicates a larger content of basaltic, Iceland-derived grains (e.g., Kaboth-Bahr et al., 2025; Mirzaloo et al., 2019). Recently, both proxies were applied at Site U1564 to infer the onset of consistently strong ISOW activity after 3.6 Ma (record spanning 2.0–5.0 Ma; Sinnesael et al., 2025). Here, we extend this record to investigate earlier fluctuations in deep water activity (5.0–6.2 Ma).

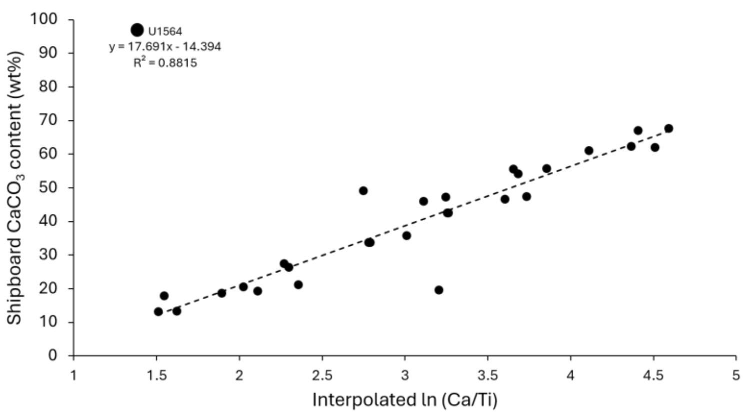

Figure 3: Calibration of $CaCO_3$ content at Site U1564. Shipboard-measured $CaCO_3$ content (wt%; Parnell-Turner et al., 2025) and XRF-derived ln(Ca/Ti) for the depths where shipboard measurements were made. A correlation coefficient R^2 = 0.8815 indicates the strong relationship between the two records and the estimated linear fit that was used to generate the high resolution $CaCO_3$ content record discussed in this study.

https://doi.org/10.5194/egusphere-2026-3764
Preprint. Discussion started: 7 July 2026

2.3 Chronostratigraphic framework and Astrochronology

An astronomically-tuned age model for the study interval (5.0–6.2 Ma) at Site U1564 was constructed by building upon the shipboard magnetostratigraphic age-depth points (Parnell-Turner et al., 2025). The availability of a complete spliced sedimentary record provided an excellent basis for a cyclostratigraphic approach and was made more robust through leveraging previously established astronomical tuning frameworks in the region (Table 1). For example, Sinnesael et al. (2025) correlated the Site U1564 magnetic susceptibility (MS) record between 2.0–5.0 Ma to the LR04 benthic $\delta^{18}O$ stack (Lisiecki and Raymo, 2005; interval 1.9–2.7Ma) and the obliquity astronomical solution (interval 2.7–5.0Ma), based on a well-documented relationship of MS to glacial–interglacial cycles (Jansen et al., 1996; Table 1). In another study, Hodell et al. (2001) generated an astronomically tuned age model for Rockall Plateau ODP Site 982 (Fig. 2), by correlating benthic foraminifera $\delta^{18}O$ to the obliquity astronomical solution, and sediment gamma ray attenuation (GRA) bulk density to summer insolation (65°N). Finally, Drury et al. (2018) recently revisited the ODP Site 982 age model and generated an astronomically tuned age model based on the correlation between benthic foraminifera $\delta^{18}O$ records and an eccentricity, tilt, anti-phased precession (ET-P) astronomical solution (La2004; Laskar et al., 2004). Since benthic foraminifera isotopic records are not yet available for Site U1564, MS is a useful alternative cyclostratigraphic proxy for age model construction.

Table 1: Summary of phase relationship assumptions and tuning strategy for previously published astronomically tuned age models in the North Atlantic area.

Orbital Target & Relative Climate	Study	Site/Interval	Oxygen Isotopes	$CaCO_3$ content	Magnetic Susceptibility	GRA density
Obliquity (High/Low) Warmer/Colder	Jansen et al.,1996; LR04	ODP 983 0–5.3 Ma	Low/High		Low/High	
	Hodell et al., 2001	ODP 982 4.6–7.5 Ma	Low/High			
	Sinnesael et al., 2025/IODP U1564	IODP U1564 1.7–5 Ma		High/Low	Low/High	
Summer Insolation 65°N (High/Low) **Precession** (Low/High) Warmer/Colder	Hodell et al., 2001	ODP 982 4.6–7.5 Ma		High/Low		High/Low
ET-P (High/Low) Warmer/Colder	Drury et al., 2018	ODP982 4.5–8 Ma	Low/High			
	This study	IODP U1564 5–6.2 Ma		High/Low	Low/High	

https://doi.org/10.5194/egusphere-2026-3764
Preprint. Discussion started: 7 July 2026

A comparison of Site U1564 MS and calibrated $CaCO_3$ content shows that the two records are strongly anti-correlated (Fig. 4), although $CaCO_3$ content has higher relative amplitude variations and more resolved cyclic changes compared to the MS signal (Fig. 4). For this reason, we decided to use the $CaCO_3$ content record for cyclostratigraphy. Based on the combination of previously established phase relationships between North Atlantic records and orbital solutions (see Table 1), $CaCO_3$ content (wt%) maxima (minima) were correlated to ET-P maxima (minima) using the open-source software package QAnalyseries (Kotov and Pälike, 2018). The astrochronology, encompassing 54 age-depth ties, which include the original magnetostratigraphic tie points, are presented in Figure 5 and Supplementary Table 1. Following that, we linearly interpolated the XRF data points between the new age-depth points to generate a highly resolved XRF time series using the tune function of R-package *astrochron* (Meyers, 2014). The astronomically-tuned age model was subsequently also used to calculate mass accumulation rates of $CaCO_3$, in g cm^{-2} kyr^{-1}, given by the Eq. (1):

$$\mathrm{CaCO3\ fluxes} = \mathrm{Calibrated\ CaCO3\ content}\ \times \mathrm{LSR}_{astro} \times \mathrm{DBD}$$

where Calibrated $CaCO_3$ content refers to the coulometry-calibrated high-resolution XRF record generated in this study (in wt%/100), LSR_{astro} refers to the linear sedimentation rates (cm/kyr) estimated between the age-depth points of the astrochronology, and DBD refers to the sediment dry bulk density. For the latter, we used the shipboard dry density (g/cm^3) measurements (Parnell-Turner et al., 2025). Specifically, two averages were calculated, each for a distinct phase of dry density (g/cm^3) in the studied interval. The transition point for these two segments was visually placed at 600 m CCSF (see Data Table 4).

The ODP Site 982 $CaCO_3$ flux record was generated using the available $CaCO_3$ content record (Diester-Haass et al., 2005), updated LSR estimates using the Drury et al. (2018) age model, and calculated dry density values for the $CaCO_3$ content sample depth. For the latter, we interpolated between available dry density measurements from ODP Hole 982B (Jansen et al., 2005). Finally, the updated ODP Site 982 $CaCO_3$ flux time series were compared to changes observed at Site U1564 across the late Miocene and early Pliocene. For the comparison of $CaCO_3$ fluxes between the two sites, the Site U1564 flux record was resampled to the specific age of the updated ODP Site 982 $CaCO_3$ flux record.

https://doi.org/10.5194/egusphere-2026-3764
Preprint. Discussion started: 7 July 2026

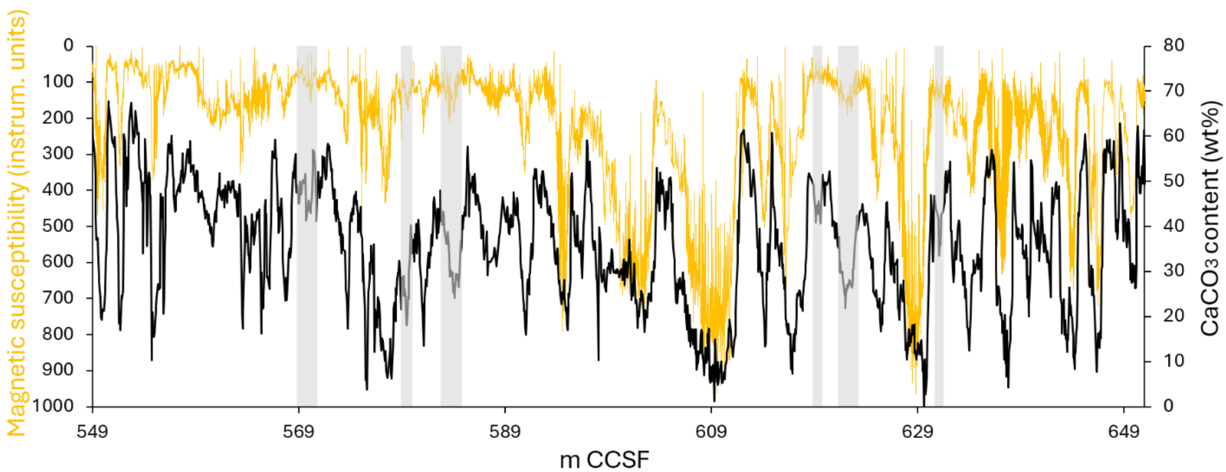

Figure 4: Time series of Site U1564 magnetic susceptibility (composite record from Holes C and D, orange line; Parnell-Turner et al., 2025) and calibrated $CaCO_3$ content (wt%; black line) plotted against m core composite depth below seafloor (CCSF). Note the reversed axis of the magnetic susceptibility record. Shaded areas indicate examples of intervals where the calibrated $CaCO_3$ content (wt%) demonstrates higher amplitude and cyclic structure that is less pronounced or completely missing in the MS record.

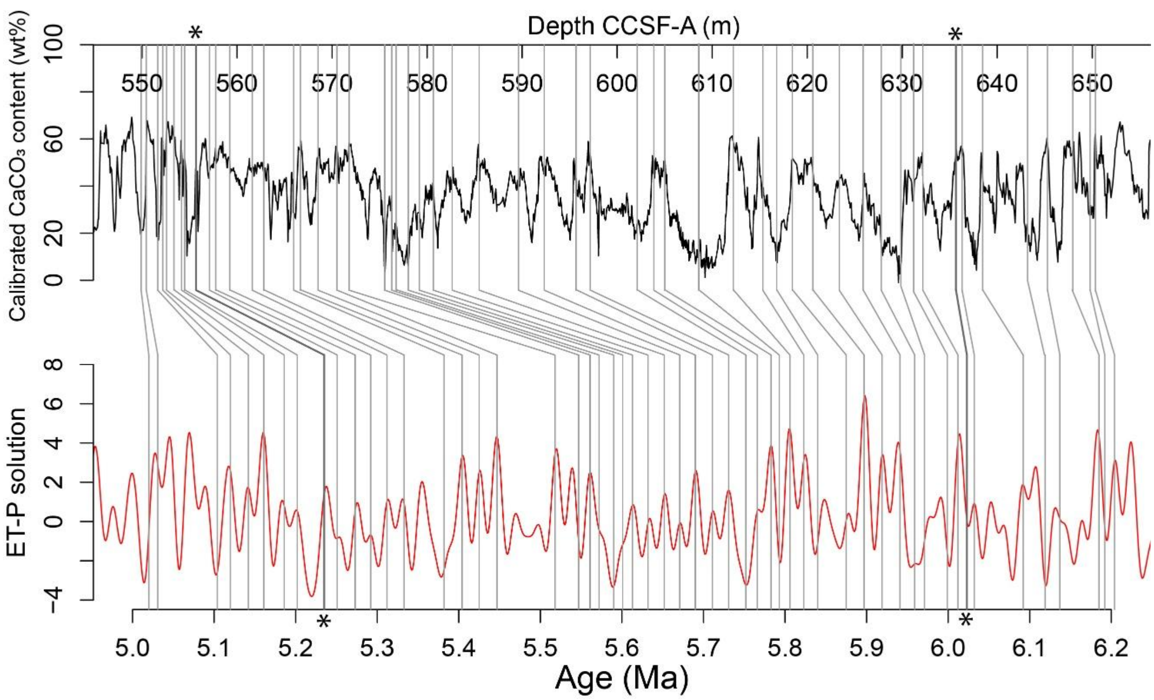

Figure 5: Astronomical tuning ties for Site U1564. Calibrated $CaCO_3$ content (wt%) record in the depth domain (m CCSF) (black line). b) ET-P (La2004; Laskar et al., 2004) orbital solution (red line). Ties with stars (*) indicate initial magnetostratigraphic tie points, which were used as baseline for cyclostratigraphy.

https://doi.org/10.5194/egusphere-2026-3764
Preprint. Discussion started: 7 July 2026

3 Results

3.1 Chronostratigraphic framework and Astrochronology

The MS and $CaCO_3$ (wt%) records are characterised by thick cycles before ~566 m CCSF (Fig. 4), which then become thinner. These thicker cycles correspond to an interval of higher accumulation rates at the site, which are then reduced, as also evidenced by the decrease in the distance between subsequent age-depth astronomical ties (Fig. 5). In Figure 6, the tuned calibrated $CaCO_3$ (wt%) time series between 3.60–6.20 Ma was compared to the ET-P solution in two sections/intervals (Fig. 6) using the astronomical tuning from Sinnesael et al., 2025 for the interval 3.60–5.00 Ma (Fig. 6a) and the astronomical tuning from this study for the interval 5.00–6.20 Ma (Fig. 5; Fig. 6b). Although different records and tuning targets were used between 3.60–5.00 Ma, the $CaCO_3$ (wt%) and the ET-P solution exhibit consistent phase and amplitude alignment in both intervals, supporting the validity of our approach and the robustness of the astronomical tuning (Fig. 6). Additionally, the $CaCO_3$ (wt%) record was compared to the benthic foraminifera $\delta^{18}O$ record from ODP Site 982 (Fig. 7a), which was independently tuned by Drury et al. (2018). Overall, this comparison also supports a good phase coherence and clear correspondence in major record shifts between the two sites and the proxies used. Specifically, we observe stepwise changes at ~5.55 Ma occurring at both records, and good alignment between distinct lows in the Site U1564 calibrated $CaCO_3$ (wt%) record (Fig. 7a) and the prominent isotopic excursions TG10/12 between 5.50–5.60 Ma and TG20/22 between 5.70–5.80 Ma (Drury et al., 2018; Shackleton et al., 1995). The consistent patterns between carbonate and isotopic records between these two North Atlantic sites further support the reliability of the tuning and the effect of common paleoclimatic mechanisms controlling deposition in the shallower and deeper parts of the region. Minor misalignments between the two records (offset of peaks of ~10–25 kyr) do occur in some intervals and likely reflect minimal errors in astronomical tuning at either location (precessional cycles) or minor hiatuses related to stronger bottom current activity at the deeper site. Nonetheless, the overall alignment for most of the record confirms the robustness of the new chronostratigraphic framework. Combined, the work from this study and Sinnesael et al. (2025), provides an astronomically tuned record for Site U1564 spanning the late Miocene to early Pleistocene. Together with ODP Site 983 (e.g, Channell et al., 2002 and references therein), the Gardar Drift is now astronomically tuned for the past ~6 Myrs.

https://doi.org/10.5194/egusphere-2026-3764
Preprint. Discussion started: 7 July 2026

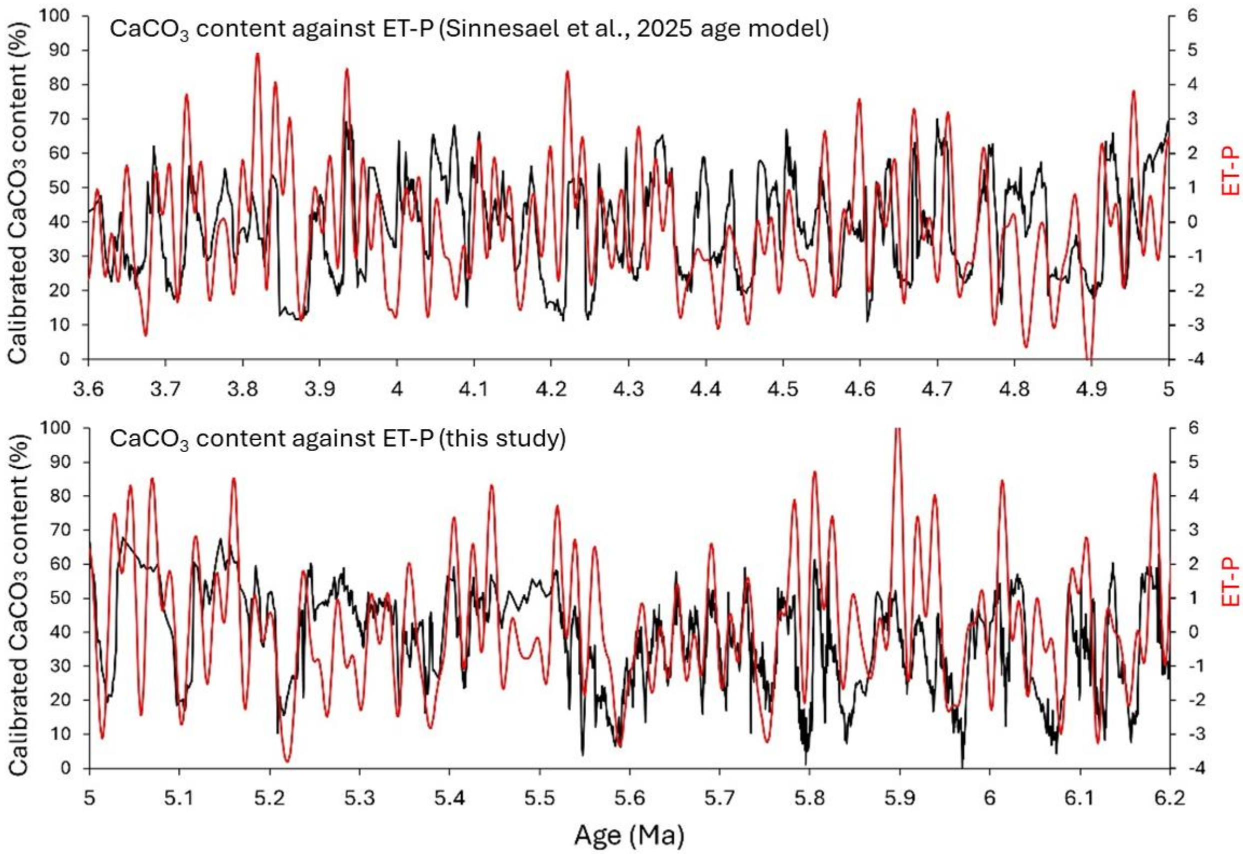

Figure 6: Calibrated $CaCO_3$ content (wt%) record against the ET-P solution (Laskar et al., 2004). The record is presented in the time domain using the astronomically tuned age model from Sinnesael et al. (2025) for the interval between 3.6–5.0 Ma, and this study for the interval between 5.0–6.2 Ma.

3.2 Sedimentation rates, XRF ratios and $CaCO_3$ content

We identify three distinct intervals between 6.20–5.00 Ma, based on a visual identification/classification of the major trends among the different records (Fig. 7), namely Interval I: 6.20–5.55 Ma, Interval II: 5.55–5.23 Ma, and Interval III: 5.23–5.00 Ma (Fig. 7). For the progressive increasing trend of carbonate content/decreasing trend of XRF proxies, which is observed roughly between 5.60–5.50 Ma (e.g., Fig. 7a,c,d), the middle point of the trend was used (5.55 Ma) to define the boundary between two intervals. Below, we describe the overall variability of the records, as well as the main changes observed across each interval transition.

Sedimentation rates average ~10 cm/kyr throughout the entire study period (6.20-5.00 Ma), with notably higher values during Interval I (~12 cm/kyr) (Fig. 7b). Following this, sedimentation rates dropped to an average of ~5 cm/kyr and remain low until 5.00 Ma (Interval II and III). Occasional sharp increases in sedimentation rates appear across Interval I, likely artificially

https://doi.org/10.5194/egusphere-2026-3764
Preprint. Discussion started: 7 July 2026

resulting from fine-tuning between two adjacent depth points (e.g., one paleomagnetic and one cyclostratigraphic tie). However, even if these peaks are excluded from the calculation of average sedimentation rates, an overall sustained shift in depositional regime seems to have occurred at 5.55 Ma (Fig. 7b) and is potentially linked to environmental or oceanographic changes.

The calibrated $CaCO_3$ (wt%) content was slightly elevated and less variable during Interval II (5.55–5.30 Ma) compared to Interval I, suggesting more stable carbonate preservation conditions or higher export production. Meanwhile $CaCO_3$ fluxes were overall higher between 6.20–6.10 Ma and 5.90–5.55 Ma and demonstrate a sustained reduction only during Interval III (Fig. 7c).

Following the patterns in sedimentation rates, the XRF elemental ratios of Zr/Rb and Ti/K show higher amplitude variability and elevated mean values during Interval I, indicating large fluctuations between stronger/weaker bottom current activity and enhanced/reduced input of Iceland-sourced terrigenous material (Fig. 7d). During Interval II, both proxies exhibit an interval of low amplitude and absolute values, reflecting a period of reduced current strength and/or sediment supply. During Interval III, three distinct peaks occurred, matching the lows in $CaCO_3$ content. These peaks correspond to transient increases in detrital input (Fig. 7d). However, they are not linked to any major perturbations in sedimentation rates, which remained low during this time.

Based on these observations, we summarize that: Interval I (6.20–5.55 Ma) was characterized by overall high and variable sedimentation rates and XRF ratios (Zr/Rb, Ti/K), as well as strong fluctuations in calibrated $CaCO_3$ content (wt%) content; Interval II (5.55–5.23 Ma) was characterized by the reduction in sedimentation rates and lower $CaCO_3$ fluxes compared to Interval I, muted amplitude of XRF proxies, and improved preservation of $CaCO_3$; Interval III (5.23–5.00 Ma) had distinct isolated minima of low $CaCO_3$ content and high terrigenous XRF ratios and, overall, had the lowest sedimentation rates and the lowest recorded $CaCO_3$ fluxes.

4 Discussion

4.1 North Atlantic bottom current activity across the latest Miocene warming

Sedimentation at Gardar Drift has been commonly linked to the activity of ISOW-related bottom currents (e.g., Langehaug et al., 2016; Hodell et al., 2009; Bianchi and McCave, 1999). Recently, it was shown that strong and persistent ISOW current activity was established in the area after 3.6 Ma, influencing Björn and Gardar Drift sites (Sinnesael et al., 2025). This transition was characterized by a ~four-fold increase (from ~4.20 before 3.6 Ma to 17 cm/kyr after) in sedimentation rates at Site U1564. By extending the record to 6.20 Ma, we show that average sedimentation rates between 6.20–5.00 Ma lie intermediate between the sedimentation rates from 5.00–3.60 Ma, when ISOW activity was not yet strengthened and 3.60–2.70 Ma, when sediment

https://doi.org/10.5194/egusphere-2026-3764
Preprint. Discussion started: 7 July 2026

supply and current strength in Gardar Drift were consistently high (Sinnesael et al., 2025). The above observations provide evidence that strong bottom currents were operating in the area as early as 6.20 Ma. However, the latest Miocene–early Pliocene activity was notably different from that observed after 3.60 Ma, since it was characterized by strong periodic fluctuations in Zr/Rb, Ti/K, and $CaCO_3$ content, as opposed to consistently high elemental ratios and a minimal contribution of the carbonate fraction between 3.60–2.70 Ma (Sinnesael et al., 2025).

We propose that the changes in relative contribution of terrigenous versus pelagic (biogenic) sediment reflect the periodic influence of distinct bottom currents and/or water masses, which acted to preferentially dilute and/or dissolve the carbonate fraction during the latest Miocene and early Pliocene. We link each interval to its corresponding dominant circulation component by using the previously established interpretations for sedimentation rates, Zr/Rb, and Ti/K at North Atlantic contourite deposition sites (e.g., Mirzaloo et al., 2019; Grützner and Higgins 2010; Toucanne et al., 2021; see also Methods). Given high Ti/K ratios and high sedimentation rates we suggest an overall stronger presence of ISOW-related bottom currents during Interval I. This presence was characterized by pulses of stronger activity and corresponds to the latest stages of the LMC (Fig. 7e). ISOW presence was then significantly reduced during Intervals II and III (Fig. 7). Specifically, during these intervals, sedimentation rates were similar to those between 5.00–3.60 Ma, a period with overall weaker ISOW-related bottom current activity (Fig. S2; Sinnesael et al., 2025). We now show that this period of weak ISOW already began at 5.55 Ma, as also evidenced by the reduced amplitude of the XRF ratios (Fig 7d). Interestingly, this timing falls very close to the end of the LMC (5.50 Ma; e.g., Holbourn et al., 2018; Herbert et al., 2016; Ao et al., 2021; Wen et al., 2023) and corresponds to the onset of the LMW, which is characterised by lighter oxygen isotopic values in the North Atlantic (ODP Site 982; Drury et al., 2018) and globally warmer SSTs (Herbert et al., 2016; Fig. 7e).

The LMW may have driven weaker overturning circulation and resulting deep-current activity through the establishment of weaker meridional (north-south) temperature gradients, which resembled the ones that persisted during the early Pliocene (Brierley and Fedorov, 2010). ISOW weakening could have also been linked to reduced deep-water convection due to freshening of the water column. This freshening can occur in the subpolar North Atlantic when ice-melt is introduced to the water column (e.g., Böning et al., 2016). The presence of substantial glaciations in south Greenland since ~7 Ma (Larsen et al., 1994) might further support that such mechanism could have been possible even before the onset and intensification of extensive Northern Hemisphere glaciations at ~3.60 and ~2.70 Ma (McClymont et al., 2023). The importance of late Miocene-Pliocene ISOW weakening as a climatic feedback mechanism should also be considered in future studies. Subpolar and polar deep-water formation in the North Atlantic makes this region one of the most efficient in CO_2 transfer from the atmosphere to the deep ocean (Takahashi et al., 2009). Slowing the rate of this deep-water formation, as inferred from ISOW weakening, would also have an impact on this air-sea gas exchange, with the potential for reduced oceanic CO_2 uptake on short timescales. However, there is substantial evidence that, on geological timescales, weaker Atlantic overturning circulation is associated with lower, not higher, atmospheric CO_2, primarily due to the build-up and dominance of less-ventilated southern-sourced

https://doi.org/10.5194/egusphere-2026-3764
Preprint. Discussion started: 7 July 2026

deep waters, that trap more respired carbon at depth and reduce CO_2 outgassing from the Southern Ocean (e.g., Sigman and Boyle, 2000; Toggweiler et al., 2006; Freeman et al., 2016). It becomes evident that more highly resolved proxy records (e.g., SST, CO_2, water mass tracers) will be needed to establish lead and lag relationships within the context of larger-scale climatic change. Furthermore, paleoclimate modelling using the newly available records will help us elucidate if the proposed mechanisms could have been physically feasible.

Regarding the overall increase in $CaCO_3$ content during Interval II (Fig. 7a), this could either reflect the reduced terrigenous component transported by bottom currents, an increase in the production of biogenic carbonate, or reduced dissolution within the water column through the influence of a less corrosive water mass. The $CaCO_3$ fluxes at ODP Site 982 have, on average, similar values to the one from U1564 (Diester-Haas et al., 2005; this study; Fig. 7c), supporting that no major, sustained change occurred in paleoproductivity or selective preservation at the deeper site during Interval II. This observation, in turn, suggests that higher $CaCO_3$ content at Site U1564 reflects less terrigenous input through a weakening of ISOW-related bottom currents, strengthening the proposed changes across this transition.

During Interval III, $CaCO_3$ fluxes between the two sites were progressively decoupled, driven by a decrease at Site U1564 and an increase at ODP Site 982 (Fig. 7c). This can be explained by the combined effect of high carbonate export production and burial related to a period of globally high paleoproductivity (known as the late Miocene to Pliocene biogenic bloom; Diester Haass et al., 2005) at the shallower site, and the presence of a more corrosive water mass at the deeper parts of the basin. The latter could occur when, in the absence of persistently strong ISOW bottom current activity, less ventilated and more corrosive southerly sourced waters were reaching the deeper parts of the North Atlantic, as suggested for glacial periods of the Pleistocene (e.g., deMenocal et al., 1997). The overall reduction of $CaCO_3$ preservation at Site U1564 could equally offer an explanation for why overall sedimentation rates remained low, despite the periodic resumption of terrigenous sediment input during Interval III. The latter short-lived pulses of stronger bottom current activity had slightly smaller amplitude than those during Interval I and did not impact the total sedimentation rates (Fig. 7b). Overall, all records during Interval III resemble the early Pliocene circulation regime between 5.00–3.60 Ma (Sinnesael et al., 2025; Fig. S2), where strong lithological variations co-exist with lower sedimentation rates. This possibly indicates that during the Early Pliocene, bottom current activity was present but wasn't strong enough to generate a consistent drift-like sedimentation regime.

In general, direct and continuous sedimentary evidence from high latitude sites under the influence of deep currents are scarce for the study period. For that reason, most of the previously described processes either come from lower latitude sites, sites outside depositional systems of drifts, or the interpretation of seismic data. Additionally, many of the interpretations in this study (including our XRF data), come from the knowledge we have acquired regarding drift deposition during the Pleistocene and the Holocene, when the climatic system was in a very different state. With these limitations in mind, we therefore discuss some studies which have inferred deep-water formation and related bottom current strength for the Miocene and early Pliocene.

https://doi.org/10.5194/egusphere-2026-3764
Preprint. Discussion started: 7 July 2026

Dausmann et al. (2017) generated radiogenic Nd records at South Atlantic ODP Site 1088, to trace the presence of North Component Water (NCW; name for the precursor of the NADW) south of the equator. Based on their analysis, NCW was being exported towards the Southern Ocean between 6.00–3.00 Ma. In another study, Müller-Michaelis and Uenzelmann-Neben (2014), synthesized detailed seismic profile observations from the Eirik drift system, which they tied to the age model from ODP Site 646 (Müller-Michaelis et al., 2013; Arthur et al., 1989). Based on the interpretation of seismic units, they proposed reduced DSOW-related sediment deposition during the latest Miocene cooling (7.50–5.60 Ma), and subsequent reinvigoration during the warming phases of the latest Miocene and early Pliocene (Müller-Michaelis and Uenzelmann-Neben, 2014 and references therein). This finding comes in contrast to the evolution of the Gardar Drift system proposed here. However, it is important to note that recently published sedimentation rates and XRF proxies from sites to the west of the Reykjanes Ridge demonstrate a very different depositional history compared to the sites on the east (e.g., Morris et al., in review; Sinnesael et al., 2025). This asymmetry could be explained by a decoupled history of the Eirik and Gardar Drifts, through differentiated DSOW and ISOW pathways during the late Miocene, similar to what has been shown for the deep-water masses to the east and west of the Reykjanes Ridge during some Holocene intervals (Hoogakker et al., 2011). Therefore, the integration of seismic data and the new sedimentological evidence is crucial to understand the evolution of both the Gardar and Eirik Drifts during the Mio-Pliocene. Such a coupled approach will reveal if what we interpret here as a late Miocene reduction in ISOW activity can be partially explained or attributed to a lateral migration of drift depocenters, short-lived changes in bottom current flow paths, or even localized weakening of an ISOW segment. Comparison with shallower and deeper sites, including the ones drilled at Björn Drift, as well as analysis of sediment provenance, will be necessary to complete the picture.

4.2 Tectonic drivers of change in deep water formation

Tectonic processes are commonly used to explain long-term paleoclimatic and paleoceanographic changes. Reconciling tectonic drivers with rapid and/or transient climatic changes remains difficult due to the differences in timescales. However, threshold behavior, or the interplay between a tectonic and a climatic process (e.g., the closure of a gateway and sea level fluctuations), can lead to sustained changes in atmospheric systems and ocean circulation dynamics. The tectonic events that could have impacted ocean circulation in the Atlantic Ocean during the late Miocene-early Pliocene are: the uplift and subsidence of the Greenland-Scotland Ridge (GSR; Poore et al., 2006), the opening of the Bering Strait (Hu et al., 2015), and the restriction of the Mediterranean with the resulting Messinian salinity crisis (MSC; Ivanovic et al., 2014). These tectonic changes have been linked to several climatic feedback mechanisms and have been proposed as direct or indirect drivers of AMOC strength and NADW (or NCW) formation.

A reduced gradient in deep ocean $\delta^{13}C$ between North and South Atlantic sites has been used to infer stronger NCW production and has been linked to subsidence at the Greenland-Scotland gateway (Parnell-Turner et al., 2015; Poore et al., 2006; Wright and Miller, 1996). Poore et al. (2006) showed that a rapid increase of NCW occurred around 6 Ma, in good agreement with

https://doi.org/10.5194/egusphere-2026-3764
Preprint. Discussion started: 7 July 2026

the first high amplitude peaks at Site U1564 Zr/Rb and Ti/K (Fig. 7d). However, the $\delta^{13}C$-derived interval of overall stronger overturning circulation spanned 6.00 to 2.50 Ma, without resolving higher frequency fluctuations in 100-kyr timescales (e.g., Parnell-Turner et al., 2015). Based on a similar approach of $\delta^{13}C$ gradients, Hodell and Venz-Curtis (2006) inferred a modern-like Atlantic Ocean circulation between 6.6–3.6 Ma, that most closely resembled the interglacial periods of the Holocene.

Another relevant tectonic reorganization is the opening of the Bering Strait, which could have affected AMOC by introducing fresher Pacific water into the Arctic Ocean and subsequently the Nordic Seas, with the later one being the area where ISOW deep water forms. Specifically, modelling studies suggest that an open Bering Strait is linked to weaker NADW (Shaffer and Bentsen, 1994) through a freshwater balance mechanism and that, vice versa, a strengthening of the AMOC follows the closure of the strait (e.g., Brierley and Fedorov, 2016; Hu et al., 2015). Interestingly, this opening has been suggested to enter a key phase between 5.6–5.4 Ma (Hall et al., 2023; Gladenkov et al., 2002), and was further confirmed by the presence of Pacific molluscs within the Iceland basin by 5.2 Ma (Hall et al., 2023). Its timing is therefore coeval with the overall weakening in bottom current activity observed during Interval II.

Another gateway-related mechanism that could have influenced bottom current activity in the North Atlantic is the isolation and re-connection of the Mediterranean Sea during the MSC. A reduction in the Mediterranean overflow water (MOW) could have ceased the salt injection into the North Atlantic, which has been proposed to affect and enhance overturning circulation in the Atlantic (see Khélifi et al., 2009, and references therein). Additionally, the MSC could have contributed to the overall late Miocene cooling of the North Atlantic Ocean, through the removal of the contribution of warm and saline MOW from the Atlantic Ocean budget (Ng et al., 2021, and references therein). Roveri and others (2025) summarizes the well-established stages of the MSC. These stages include: a complete MOW shutdown between 5.62–5.55 Ma, and a complete isolation of the Mediterranean from the Atlantic between 5.55–5.33 Ma, before the MSC ended and connectivity was re-established. These stages of halted MOW, which have been shown to result from eustatic changes during glacial stages TG14/TG12 (Roveri et al., 2014, Hilgen et al., 2007; Fig. 7a) fall close to (and slightly predate) the onset of weaker ISOW during Interval II (5.55 Ma). Additionally, the end of the MSC at 5.33 Ma falls close to the resumption of the periodical pulses of deep current activity at Site U1564, which are observed during Interval III (5.25 Ma), suggesting a possible MOW effect on overturning circulation. However, although various evidence, such as drift deposition and benthic foraminifera assemblage changes at the Iberian margin support an active Mediterranean-Atlantic exchange and deep-current activity right after the MSC (García-Gallardo et al., 2017; Hernández-Molina et al., 2016), a regular presence of MOW was not established in the North Atlantic before 4.5 Ma (e.g., Hernández-Molina et al., 2014 and references therein).

Taken together, the ISOW weakening during Interval II could have been tectonically driven or enhanced through a combined effect of the Bering Strait restriction of the Mediterranean, while the resumption of deep current activity during Interval III could have been assisted by the resumption of MOW. Regardless of MOW activity, carbonate dissolution in the deeper parts

https://doi.org/10.5194/egusphere-2026-3764
Preprint. Discussion started: 7 July 2026

of the basin suggests that southerly sourced water masses were being entrained in the North Atlantic during this interval. The above mechanisms will need to be supported by isotopic and micropaleontological proxy evidence used in past water mass tracing, as well as assessed through paleoclimatic ocean circulation modelling.

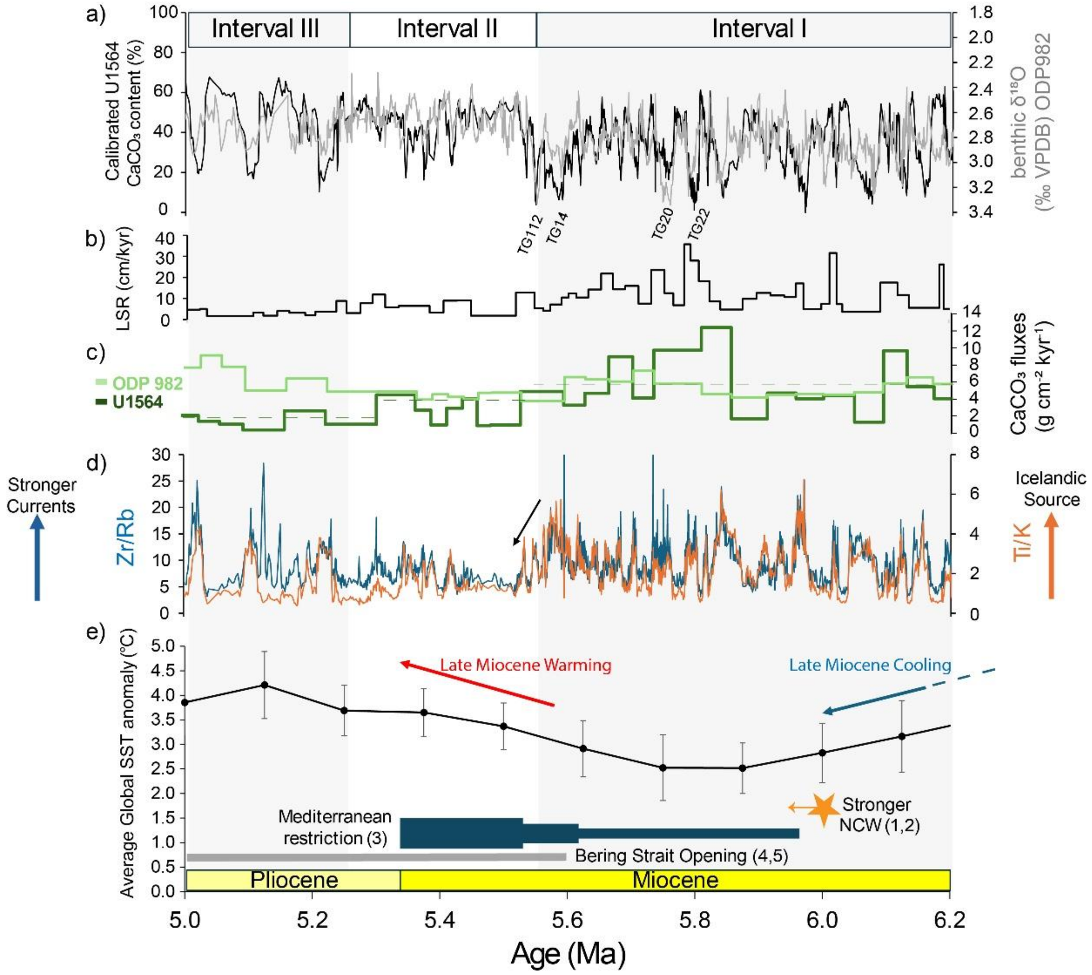

Figure 7: Bottom current activity, paleoclimatic conditions and tectonic reconfigurations across the latest Miocene and early Pliocene. a) Astronomically tuned and calibrated $CaCO_3$ content (wt%) record (black line) at Site U1564 (this study), plotted together with the $\delta^{18}O$ record from Drury et al., 2018 (grey line). Good overall alignment across main record features supports the robustness of the astronomically tuned age model. Also indicated are major positive isotopic excursions (isotopic stages TG20/TG22 and TG12/TG14). b) Sedimentation rates at U1564 derived from age-depth points of the astronomically tuned age model. c) $CaCO_3$ fluxes (g cm^{-2} kyr^{-1}) at Site U1564 (dark green line) and at ODP Site 982 (light green line; Diester-Haass et al., 2005). For the latter, ages are updated to the Drury et al., (2018) age model. Horizontal dashed lines indicate the average $CaCO_3$ fluxes at U1564 during Intervals I-III. d) XRF derived Zr/Rb (orange) and Ti/K (blue) time series at Site U1564, presented in the astronomically tuned age model. e) Compiled globally averaged Sea Surface Temperature (SST) anomaly relative to today (Data Table 6; initial data from Herbert et al., 2016). Orange star with arrow: The beginning of stronger NCW as suggested by Wright and Miller 1996 (1) and Poore et al., 2006 (2); Blue bars: Restriction of the Mediterranean as summarized in Roveri et al., 2025 (3); Gray bar: Bering Strait opening as proposed by Hall et al., 2023 (4) and Gladenkov et al., 2002 (5).

https://doi.org/10.5194/egusphere-2026-3764
Preprint. Discussion started: 7 July 2026

5 Conclusions

The combination of astronomically tuned sedimentological, XRF and $CaCO_3$ content records at Site U1564 allows us to extend the reconstruction of bottom current activity and $CaCO_3$ preservation at Gardar Drift back to 6.2 Ma. Based on the combination of proxies, three main intervals were identified (Intervals I-III). During Interval I (6.20–5.55 Ma), ISOW activity was more pronounced and demonstrated stronger fluctuations. This interval corresponds to the last stages of the LMC. Interval II (5.55–5.23 Ma) was characterized by muted amplitude of XRF elemental ratios and lower sedimentation rates, as well as higher carbonate content. It corresponds to the LMW, as well as the final stages of the MSC and the opening of Bering Strait, suggesting that a combination of globally warmer conditions and tectonic reorganizations around the Atlantic Ocean gateways possibly drove the observed patterns. Finally, during Interval III (5.23–5.00 Ma), after the warm Pliocene conditions were established, periodic changes in lithology resumed and sedimentation rates and style of depositions remained stable until the onset of strong ISOW at 3.6 Ma. During this interval, there are indications that corrosive, southerly sourced waters were reaching the deeper parts of the basin. More data, including upper ocean and bottom ocean stable isotopes, SST reconstructions and assemblage studies from the species contributing to the carbonate production will be needed to further substantiate the proposed oceanic regime changes.

Code and data availability

The supporting data for this study have been deposited in Zenodo and will become publicly available upon publication at: 10.5281/zenodo.20849518

Supplement link

The link to the supplement will be included by Copernicus, if applicable.

Author contributions

A.B. and R.P.-T. served as chief scientists, and L.L. as staff scientist, during IODP Expedition 395. B.Th.K. conceived the study, compiled and synthesized the data, prepared the figures, and wrote the manuscript. M.S. assisted with data interpretation and age-model generation. H.S. contributed to map and profile generation, while M.M. processed and cleaned the XRF data. T.D.J. contributed to data interpretation and manuscript writing. P.C. provided supervision and project administration. A.J.D., P.N.P., E.H., S.R.H., C.J., A.D.C., S.S., S.F., and D.D. reviewed and edited the manuscript. All authors provided feedback at various stages of the manuscript writing process.

https://doi.org/10.5194/egusphere-2026-3764
Preprint. Discussion started: 7 July 2026

Competing interests

The authors declare that they have no conflict of interest.

Acknowledgements

This research used data related to International Ocean Discovery Program Expedition 395 and Ocean Drilling Program Leg 162. We would therefore like to acknowledge all the JOIDES Resolution scientists, staff members, crew, drillers, as well as the repository technicians and curators for their tireless work that makes all our research possible. We would also like to acknowledge the IODP Exp 395 scientists that contributed to the XRF scanning of the U1564 cores.

Financial support

The project received funding from the European Union's Horizon 2020 research and innovation program under the Marie Skłodowska-Curie grant agreement No 945380 to BTK and was hosted by the AMGC group at Vrije Universiteit Brussel under the supervision of Philippe Claeys. SS research was funded through MUR for ECORD-IODP Italia. PC acknowledges support from VUB Strategic Research Program & VUB Large Research Group Funding.

https://doi.org/10.5194/egusphere-2026-3764
Preprint. Discussion started: 7 July 2026

References

Amante, C. and Eakins, B. W.: ETOPO1 1 Arc-Minute Global Relief Model: Procedures, Data Sources and Analysis, NOAA Technical Memorandum NESDIS NGDC-24, National Geophysical Data Center, NOAA, https://doi.org/10.7289/V5C8276M, 2009.

Ao, H., Rohling, E. J., Zhang, R., Roberts, A. P., Holbourn, A. E., Ladant, J.-B., Dupont-Nivet, G., Kuhnt, W., Zhang, P., Wu, F., Dekkers, M. J., Liu, Q., Liu, Z., Xu, Y., Poulsen, C. J., Licht, A., Sun, Q., Chiang, J. C. H., Liu, X., Wu, G., Ma, C., Zhou, W., Jin, Z., Li, X., Li, X., Peng, X., Qiang, X., and An, Z.: Global warming-induced Asian hydrological climate transition across the Miocene–Pliocene boundary, Nat. Commun., 12, 6935, https://doi.org/10.1038/s41467-021-27054-5, 2021.

Arthur, M.A., Srivastava, S.P., Kaminski, M., Jarrard, R.D., Osler, J., 1989. Seismic stratigraphy and history of deep circulation and sediment drift development in Baffin Bay and the Labrador Sea. In: Srivastava, S.P., Arthur, M., Clement, B., et al. (Eds.), Proceedings of the Ocean Drilling Program, Scientific Results, vol. 105, College Station, TX, pp. 957–988

Bell, D., Jung, S., Kroon, D., Hodell, D. A., Lourens, L. J., and Raymo, M. E.: Atlantic deep-water response to the early Pliocene shoaling of the Central American Seaway, Sci. Rep., 5, 12252, https://doi.org/10.1038/srep12252, 2015.

Bianchi, G. G. and McCave, I. N.: Holocene periodicity in North Atlantic climate and deep-ocean flow south of Iceland, Nature, 397, 515–517, https://doi.org/10.1038/17362, 1999.

Bianchi, G. G. and McCave, I. N.: Hydrography and sedimentation under the deep western boundary current on Björn and Gardar Drifts, Iceland Basin, Mar. Geol., 165 (1–4), 137–169, https://doi.org/10.1016/S0025-3227(99)00139-5, 2000.

Billups, K., Ravelo, A. C., and Zachos, J. C.: Early Pliocene deep-water circulation in the western equatorial Atlantic: Implications for high-latitude climate change, Paleoceanography, 13 (1), 84–95, https://doi.org/10.1029/97PA02995, 1998.

Böning, C., Behrens, E., Biastoch, Getzlaff, A. K., and Bamber, J. L.: Emerging impact of Greenland meltwater on deepwater formation in the North Atlantic Ocean, Nature Geosci., 9, 523–527 (2016), https://doi.org/10.1038/ngeo2740, 2016.

Brierley, C. M. and Fedorov, A. V.: Relative importance of meridional and zonal sea surface temperature gradients for the onset of the ice ages and Pliocene–Pleistocene climate evolution, Paleoceanography, 25, PA2214, https://doi.org/10.1029/2009PA001809, 2010.

Burke, K. D., Williams, J. W., Chandler, M. A., Haywood, A. M., Lunt, D. J., and Otto-Bliesner, B. L.: Pliocene and Eocene provide best analogs for near-future climates, Proc. Natl. Acad. Sci. U.S.A., 115 (52), 13288–13293, https://doi.org/10.1073/pnas.1809600115, 2018.

Channell, J. E. T., Mazaud, A., Sullivan, P., Turner, S., and Raymo, M. E.: Geomagnetic excursions and paleointensities in the Matuyama Chron at Ocean Drilling Program Sites 983 and 984 (Iceland Basin), J. Geophys. Res., 107(B6), https://doi.org/10.1029/2001JB000491, 2002.

Dausmann, V., Frank, M., Gutjahr, M., and Rickli, J.: Glacial reduction of AMOC strength and long-term transition in weathering inputs into the Southern Ocean since the mid-Miocene: Evidence from radiogenic Nd and Hf isotopes, Paleoceanography, 32, 265–283, https://doi.org/10.1002/2016PA003056, 2017.

de Azevedo, A. Q., Jiménez-Espejo, F. J., Bulian, F., Sierro, F. J., Tangunan, D., Takashimizu, Y., Albuquerque, A. L. S., Kubota, K., Escutia, C., Norris, R. D., Hemming, S. R., and Hall, I. R.: Orbital forcing and evolution of the Southern African Monsoon from Late Miocene to early Pliocene, Paleoceanogr. Paleoclimatol., 38, e2022PA004588, https://doi.org/10.1029/2022PA004588, 2023.

https://doi.org/10.5194/egusphere-2026-3764
Preprint. Discussion started: 7 July 2026

deMenocal, P., Archer, D., and Leth, P.: Pleistocene variations in deep Atlantic circulation and calcite burial between 1.2 and 0.6 Ma: A combined data-model approach. In: Shackleton, N.J., Curry, W.B., Richter, C., Bralower, T.J. (Eds.), Proceedings of the Ocean Drilling Program, Scientific Results, 154, Ocean Drilling Program, College Station, TX, pp. 285–297. https://doi.org/10.2973/odp.proc.sr.154.113.1997, 1997

Diester-Haass, L., Billups, K., and Emeis, K. C.: In search of the late Miocene–early Pliocene "biogenic bloom" in the Atlantic Ocean (Ocean Drilling Program Sites 982, 925, and 1088), Paleoceanography, 20, PA4001, https://doi.org/10.1029/2005PA001139, 2005.

Drury, A. J., Liebrand, D., Westerhold, T., Beddow, H. M., Hodell, D. A., Rohlfs, N., Wilkens, R. H., Lyle, M., Bell, D. B., Kroon, D., Pälike, H., and Lourens, L. J.: Climate, cryosphere and carbon cycle controls on Southeast Atlantic orbital-scale carbonate deposition since the Oligocene (30–0 Ma), Clim. Past, 17, 2091–2117, https://doi.org/10.5194/cp-17-2091-2021, 2021.

Drury, A. J., Westerhold, T., Hodell, D., and Röhl, U.: Reinforcing the North Atlantic backbone: revision and extension of the composite splice at ODP Site 982, Clim. Past, 14, 321–338, https://doi.org/10.5194/cp-14-321-2018, 2018.

Fedorov, A. V., Brierley, C. M., Lawrence, K. T., Liu, Z., Dekens, P. S., and Ravelo, A. C.: Patterns and mechanisms of early Pliocene warmth, Nature, 496, 43–49, https://doi.org/10.1038/nature12003, 2013.

Foster, G. L., Hull, P., Lunt, D. J., and Zachos, J. C.: Placing our current 'hyperthermal' in the context of rapid climate change in our geological past, Phil. Trans. R. Soc. A, 376 (2130), 20170086, https://doi.org/10.1098/rsta.2017.0086, 2018.

Freeman, E., Skinner, L. C., Waelbroeck, C., and Hodell, D.: Radiocarbon evidence for enhanced respired carbon storage in the Atlantic at the Last Glacial Maximum, Nat. Commun., 7, 11998, https://doi.org/10.1038/ncomms11998, 2016.

García-Gallardo, Á., Grunert, P., Van der Schee, M., Sierro, F. J., Jiménez-Espejo, F. J., Alvarez Zarikian, C. A., and Piller, W. E.: Benthic foraminifera-based reconstruction of the first Mediterranean-Atlantic exchange in the early Pliocene Gulf of Cadiz, Palaeogeogr. Palaeoclimatol. Palaeoecol., 472, 93–107, https://doi.org/10.1016/j.palaeo.2017.02.009, 2017.

Gladenkov, A. Y., Oleinik, A. E., Marincovich Jr., L., and Barinov, K. B.: A refined age for the earliest opening of Bering Strait, Palaeogeogr. Palaeoclimatol. Palaeoecol., 183 (3–4), 321–328, https://doi.org/10.1016/S0031-0182(02)00249-3, 2002.

Grützner, J. and Higgins, S. M.: Threshold behavior of millennial scale variability in deep water hydrography inferred from a 1.1 Ma long record of sediment provenance at the southern Gardar Drift, Paleoceanography, 25, PA4204, https://doi.org/10.1029/2009PA001873, 2010.

Hall, J. R., Allison, M. S., Papadopoulos, M. T., Barfod, D. N., and Jones, S. M.: Timing and consequences of Bering Strait opening: New insights from 40Ar/39Ar dating of the Barmur Group (Tjörnes Beds), northern Iceland, Paleoceanogr. Paleoclimatol., 38, e2022PA004539, https://doi.org/10.1029/2022PA004539, 2023.

Haug, G. H. and Tiedemann, R.: Effect of the formation of the Isthmus of Panama on Atlantic Ocean thermohaline circulation, Nature, 393, 673–676, https://doi.org/10.1038/31447, 1998.

Haywood, A. M., Dowsett, H. J., Dolan, A. M., Rowley, D., Abe-Ouchi, A., Otto-Bliesner, B., Chandler, M. A., Hunter, S. J., Lunt, D. J., Pound, M., and Salzmann, U.; The Pliocene Model Intercomparison Project (PlioMIP) Phase 2: scientific objectives and experimental design, Clim. Past, 12, 663–675, https://doi.org/10.5194/cp-12-663-2016, 2016.

Herbert, T. D., Lawrence, K. T., Tzanova, A., Peterson, L. C., Caballero-Gill, R., and Kelly, C. S.: Late Miocene global cooling and the rise of modern ecosystems, Nature Geosci., 9, 843–847, https://doi.org/10.1038/ngeo2813, 2016.

https://doi.org/10.5194/egusphere-2026-3764
Preprint. Discussion started: 7 July 2026

Hernández-Molina, F. J., Sierro, F. J., Llave, E., Roque, C., Stow, D. A. V., Williams, T., Lofi, J., Van der Schee, M., Arnáiz, A., Ledesma, S., Rosales, C., Rodríguez-Tovar, F. J., Pardo-Igúzquiza, E., and Brackenridge, R. E.: Evolution of the Gulf of Cadiz margin and southwest Portugal contourite depositional system: Tectonic, sedimentary and paleoceanographic implications from IODP Expedition 339, Mar. Geol., 377, 7–39, https://doi.org/10.1016/j.margeo.2015.09.013, 2016.

Hernández-Molina, F. J., Stow, D. A. V., Alvarez-Zarikian, C. A., Acton, G., Bahr, A., Balestra, B., Ducassou, E., Flood, R., Flores, J.-A., Furota, S., Grunert, P., Hodell, D., Jimenez-Espejo, F., Kim, J. K., Krissek, L., Kuroda, J., Li, B., Llave, E., Lofi, J., Lourens, L., Miller, M., Nanayama, F., Nishida, N., Richter, C., Roque, C., Pereira, H., Sanchez Goñi, M. F., Sierro, F. J., Singh, A. D., Sloss, C., Takashimizu, Y., Tzanova, A., Voelker, A., Williams, T., and Xuan, C.: Onset of Mediterranean outflow into the North Atlantic, Science, 344 (6189), 1244–1250, https://doi.org/10.1126/science.1251306, 2014.

Hilgen, F. J., Kuiper, K., Krijgsman, W., Snel, E., and van der Laan, E.: Astronomical tuning as the basis for high resolution chronostratigraphy: the intricate history of the Messinian Salinity Crisis, Stratigraphy, 4 (2–3), 231–238, 2007.

Hodell, D. A., Curtis, J. H., Sierro, F. J., and Raymo, M. E.: Correlation of Late Miocene to Early Pliocene sequences between the Mediterranean and North Atlantic, Paleoceanography, 16 (2), 164–178, https://doi.org/10.1029/1999PA000487, 2001.

Hodell, D. A. and Venz-Curtis, K. A.: Late Neogene history of deepwater ventilation in the Southern Ocean, Geochemistry, Geophysics, Geosystems, 7, Q09001, https://doi.org/10.1029/2005GC001211, 2006.

Hodell, D. A., Minth, E. K., Curtis, J. H., McCave, I. N., Hall, I. R., Channell, J. E. T., and Xuan, C.: Surface and deep-water hydrography on Gardar Drift (Iceland Basin) during the last interglacial period, Earth Planet. Sci. Lett., 288 (1–2), 10–19, https://doi.org/10.1016/j.epsl.2009.08.040, 2009.

Holbourn, A. E., Kuhnt, W., Clemens, S. C., Kochhann, K. G. D., Jöhnck, J., Lübbers, J., and Andersen, N.: Late Miocene climate cooling and intensification of southeast Asian winter monsoon, Nat. Commun., 9, 1584, https://doi.org/10.1038/s41467-018-03950-1, 2018.

Hoogakker, B. A. A., Chapman, M. R., McCave, I. N., Hillaire-Marcel, C., Ellison, C. R. W., Hall, I. R., and Telford, R. J.: Dynamics of North Atlantic Deep Water masses during the Holocene, Paleoceanography, 26, PA4214, https://doi.org/10.1029/2011PA002155, 2011.

Hu, A., Meehl, G. A., Han, W., Otto-Bliesner, B., Abe-Ouchi, A., and Rosenbloom, N.: Effects of the Bering Strait closure on AMOC and global climate under different background climates, Prog. Oceanogr., 132, 174–196, https://doi.org/10.1016/j.pocean.2014.02.004, 2015.

Ivanovic, R. F., Valdes, P. J., Flecker, R., and Gutjahr, M.: Modelling global-scale climate impacts of the late Miocene Messinian Salinity Crisis, Clim. Past, 10, 607–622, https://doi.org/10.5194/cp-10-607-2014, 2014.

Jansen, E., Blum, P., and Shipboard Scientific Party: Moisture and density measured on ODP Hole 162-982B [dataset], PANGAEA, https://doi.org/10.1594/PANGAEA.258711, 2005.

Jansen, E., Raymo, M. E., Blum, P., et al., 1996.: Proc. ODP, Init. Repts., 162, College Station, TX (Ocean Drilling Program), 91–138, https://doi.org/10.2973/odp.proc.ir.162.104.1996, 1996.

Kaboth-Bahr, S., Bahr, A., Blaser, P., Voelker, A. H. L., Lippold, J., Gutjahr, M., Hodell, D. A., Channell, J. E. T., de Vernal, A., and Hillaire-Marcel, C.: Reconstruction of deep-water undercurrent variability from the outer Labrador Sea during the past 550,000 years, Quat. Sci. Adv, 17, 100266, https://doi.org/10.1016/j.qsa.2025.100266, 2025.

Karas, C., Nürnberg, D., Bahr, A., Groeneveld, G., Herrle, J. O., Tiedemann, R., and de Menocal, P. B.: Pliocene oceanic seaways and global climate, Sci. Rep., 7, 39842, https://doi.org/10.1038/srep39842, 2017.

Key, R. M., Olsen, A., van Heuven, S., Lauvset, S. K., Velo, A., Lin, X., Schirnick, C., Kozyr, A., Tanhua, T., Hoppema, M., Jutterström, S., Steinfeldt, R., Jeansson, E., Ishii, M., Perez, F. F., and Suzuki, T.: Global Ocean Data Analysis Project, Version 2 (GLODAPv2), ORNL/CDIAC-162, NDP-093, Carbon Dioxide Information Analysis Center, Oak Ridge National Laboratory, US Department of Energy, Oak Ridge, Tennessee, https://doi.org/10.3334/CDIAC/OTG.NDP093_GLODAPv2, 2015.

Khélifi, N., Sarnthein, M., Andersen, A., Blanz, T., Frank, M., Garbe-Schönberg, D., Haley, B. A., Stumpf, R., and Weinelt, M.: A major and long-term Pliocene intensification of the Mediterranean outflow, 3.5–3.3 Ma ago, Geology, 37 (9), 811–814, https://doi.org/10.1130/G30058A.1, 2009.

Kotov, S., and Pälike, H.: QAnalySeries – a cross-platform time series tuning and analysis tool. Earth and Space Science Open Archive, https://doi.org/10.1002/essoar.10500226.1, 2018.

Krijgsman, W., Hilgen, F. J., Raffi, I., Sierro, F. J., and Wilson, D. S.: Chronology, causes and progression of the Messinian salinity crisis, Nature, 400, 652–655, https://doi.org/10.1038/23231, 1999.

Lamy, F., Arz, H. W., Kilian, R., Lange, C. B., Lembke-Jene, L., Wengler, M., Kaiser, J., Baeza-Urrea, O., Hall, I. R., Harada, N., and Tiedemann, R.: Glacial reduction and millennial-scale variations in Drake Passage throughflow, Proc. Natl. Acad. Sci. U.S.A., 112 (44), 13496–13501, https://doi.org/10.1073/pnas.1509203112, 2015.

Langehaug, H. R., T. Mjell, L., Otterå, O. H., Eldevik, T., Ninnemann, U. S., and Kleiven, H. F.: On the reconstruction of ocean circulation and climate based on the “Gardar Drift”, Paleoceanography, 31, 399–415, https://doi.org/10.1002/2015PA002920, 2016.

Larsen, H. C., Saunders, A. D., Clift, P. D., Beget, J., Wei, W., and Spezzaferri, S.: Seven million years of glaciation in Greenland, Science, 264 (5161), 952–955, https://doi.org/10.1126/science.264.5161.952, 1994.

Laskar, J., Robutel, P., Joutel, F., Gastineau, M., Correia, A. C. M., and Levrard, B.: A long-term numerical solution for the insolation quantities of the Earth, Astron. Astrophys., 428 (1), 261–285, https://doi.org/10.1051/0004-6361:20041335, 2004.

Lauvset, S. K., Lange, N., Tanhua, T., Bittig, H. C., Olsen, A., Kozyr, A., Álvarez, M., Azetsu-Scott, K., Brown, P. J., Carter, B. R., Cotrim da Cunha, L., Hoppema, M., Humphreys, M. P., Ishii, M., Jeansson, E., Murata, A., Müller, J. D., Pérez, F. F., Schirnick, C., Steinfeldt, R., Suzuki, T., Ulfsbo, A., Velo, A., Woosley, R. J., and Key, R. M.: The annual update GLODAPv2.2023: the global interior ocean biogeochemical data product, Earth Syst. Sci. Data, 16, 2047–2072, https://doi.org/10.5194/essd-16-2047-2024, 2024.

Lauvset, S. K., Lange, N., Tanhua, T., Bittig, H. C., Olsen, A., Kozyr, A., Alin, S., Álvarez, M., Azetsu-Scott, K., Barbero, L., Becker, S., Brown, P. J., Carter, B. R., da Cunha, L. C., Feely, R. A., Hoppema, M., Humphreys, M. P., Ishii, M., Jeansson, E., Jiang, L. Q., Jones, S. D., Lo Monaco, C., Murata, A., Müller, J. D., Pérez, F. F., Pfeil, B., Schirnick, C., Steinfeldt,R., Suzuki, T., Tilbrook, B., Ulfsbo, A., Velo, A., Woosley, R. J., and Key, R. M.: GLODAPv2.2022: the latest version of the global interior ocean biogeochemical data product, Earth Syst. Sci. Data, 14, 5543–5572, https://doi.org/10.5194/essd-14-5543-2022, 2022.

Liebrand, D., Beddow, H. M., Lourens, L. J., Pälike, H., Raffi, I., Bohaty, S. M., Hilgen, F. J., Saes, M. J. M., Wilson, P. A., Van Dijk, A. E., Hodell, D. A., Kroon, D., Huck, C. E., and Batenburg, S. J.: Cyclostratigraphy and eccentricity tuning of the early Oligocene through early Miocene (30.1–17.1 Ma): *Cibicides mundulus* stable oxygen and carbon isotope records from Walvis Ridge Site 1264, Earth Planet. Sci. Lett., 450, 392–405, https://doi.org/10.1016/j.epsl.2016.06.007, 2016.

https://doi.org/10.5194/egusphere-2026-3764
Preprint. Discussion started: 7 July 2026

Lisiecki, L. E. and Raymo, M. E.: A Pliocene–Pleistocene stack of 57 globally distributed benthic δ18O records, Paleoceanography, 20, PA1003, https://doi.org/10.1029/2004PA001071, 2005.

Liu, M. and Tanhua, T.: Water masses in the Atlantic Ocean: characteristics and distributions, Ocean Sci., 17, 463–486, https://doi.org/10.5194/os-17-463-2021, 2021.

Loutre, M.F., and Berger, A.: Marine Isotope Stage 11 as an analogue for the present interglacial, Global Planet. Change, 36 (3), 209–217, https://doi.org/10.1016/S0921-8181(02)00186-8, 2003.

McClymont, E. L., Ho, S. L., Ford, H. L., Bailey, I., Berke, M. A., Bolton, C. T., De Schepper, S., Grant, G. R., Groeneveld, J., Inglis, G. N., Karas, C., Patterson, M. O., Swann, G. E. A., Thirumalai, K., White, S. M., Alonso-Garcia, M., Anand, P., Hoogakker, B. A. A., Littler, K., Petrick, B. F., Risebrobakken, B., Abell, J. T., Crocker, A. J., de Graaf, F., Feakins, S. J., Hargreaves, J. C., Jones, C. L., Markowska, M., Ratnayake, A. S., Stepanek, C., Tangunan, D., Climate evolution through the onset and intensification of Northern Hemisphere Glaciation, Rev. Geophys., 61, e2022RG000793, https://doi.org/10.1029/2022RG000793, 2023.

Meyers, S. R.: Astrochron: An R package for astrochronology, http://cran.r-project.org/package=astrochron, 2014.

Mirzaloo, M., Nürnberg, D., Kienast, M., and van der Lubbe, H. J. L.: Synchronous changes in sediment transport and provenance at the Iceland–Faroe Ridge linked to millennial climate variability from 55 to 6 ka BP, Geochem. Geophys. Geosyst., 20, 4184–4201, https://doi.org/10.1029/2019GC008298, 2019.

Morris, M., R. Parnell-Turner, K. Hochmuth, D. McNamara, A. Briais, L. LeVay, A. Di Chiara, T. Dunkley Jones, B. Karatsolis, P. Pearson, M. Sinnesael, and the IODP Expedition 395 Scientists (in review): Middle Miocene intensification of the Deep Western Boundary Current offshore Eastern Greenland.

Müller-Michaelis, A., and Uenzelmann-Neben, G.: Development of the Western Boundary Undercurrent at Eirik Drift related to changing climate since the early Miocene, Deep Sea Res. I, 93, 21–34, https://doi.org/10.1016/j.dsr.2014.07.010, 2014.

Müller-Michaelis, A., Uenzelmann-Neben, G., and Stein, R.: A revised Early Miocene age for the instigation of the Eirik Drift, offshore southern Greenland: Evidence from high-resolution seismic reflection data, Marine Geol., 340, 1–15, https://doi.org/10.1016/j.margeo.2013.04.012, 2013.

Ng, Z. L., Hernández-Molina, F. J., Duarte, D., Sierro, F. J., Ledesma, S., Rogerson, M., Llave, E., Roque, C., and Manar, M. A.: Latest Miocene restriction of the Mediterranean Outflow Water: a perspective from the Gulf of Cádiz, Geo-Mar. Lett., 41, 23, https://doi.org/10.1007/s00367-021-00693-9, 2021.

Olafsson, J., Olafsdottir, S. R., Takahashi, T., Danielsen, M., and Arnarson, T. S.: Enhancement of the North Atlantic CO_2 sink by Arctic Waters, Biogeosciences, 18 (5), 1689–1701, https://doi.org/10.5194/bg-18-1689-2021, 2021.

Olsen, A., Key, R. M., van Heuven, S., Lauvset, S. K., Velo, A., Lin, X., Schirnick, C., Kozyr, A., Tanhua, T., Hoppema, M., Jutterström, S., Steinfeldt, R., Jeansson, E., Ishii, M., Pérez, F. F., and Suzuki, T.: The Global Ocean Data Analysis Project version 2 (GLODAPv2) – an internally consistent data product for the world ocean, Earth Syst. Sci. Data, 8, 297–323, https://doi.org/10.5194/essd-8-297-2016, 2016.

Olsen, A., Lange, N., Key, R. M., Tanhua, T., Alvarez, M., Becker, S., Bittig, H. C., Carter, B. R., da Cunha, L. C., Feely, R. A., van Heuven, S., Hoppema, M., Ishii, M., Jeansson, E., Jones, S. D., Jutterström, S., Karlsen, M. K., Kozyr, A., Lauvset, S. K., Lo Monaco, C., Murata, A., Perez, F. F., Pfeil, B., Schirnick, C., Steinfeldt, R., Suzuki, T., Telszewski, M., Tilbrook, B., Velo, A., and Wanninkhof, R.: GLODAPv2.2019-an update of GLODAPv2, Earth Syst. Sci. Data, 11, 1437–1461, https://doi.org/10.5194/essd-11-1437-2019, 2019.

https://doi.org/10.5194/egusphere-2026-3764
Preprint. Discussion started: 7 July 2026

Olsen, A., Lange, N., Key, R. M., Tanhua, T., Bittig, H., Kozyr, A., Álvarez, M., Azetsu-Scott, K., Becker, S., Brown, P. J., Carter, B. R., da Cunha, L. C., Feely, R. A., van Heuven, S., Hoppema, M., Ishii, M., Jeansson, E., Jutterström, S., Landa, C. S., Lauvset, S. K., Michaelis, P., Murata, A., Pérez, F. F., Pfeil, B., Schirnick, C., Steinfeldt, R., Suzuki, T., Tilbrook, B., Velo, A., Wanninkhof, R., and Woosley, R. J.: GLODAPv2.2020 - the second update of GLODAPv2, Earth Syst. Sci. Data, 12, 3653–3678, https://doi.org/10.5194/essd-12-3653-2020, 2020.

Orvik, K. A., and P.Niiler: Major pathways of Atlantic water in the northern North Atlantic and Nordic Seas toward Arctic, Geophys. Res. Lett., 29 (19), 1896, https://doi.org/10.1029/2002GL015002, 2002.

Parnell-Turner, R. E., Briais, A., LeVay, L. J., and Expedition 395 Scientists: Reykjanes Mantle Convection and Climate, Proceedings of the International Ocean Discovery Program. International Ocean Discovery Program. https://doi.org/10.14379/iodp.proc.395.2025, 2025.

Parnell-Turner, R., White, N. J., McCave, I. N., Henstock, T. J., Murton, B., and Jones, S. M.: Architecture of North Atlantic contourite drifts modified by transient circulation of the Icelandic mantle plume, Geochem. Geophys. Geosyst., 16, 3414–3435, https://doi.org/10.1002/2015GC005947, 2015.

Poore, H. R., Samworth, R., White, N. J., Jones, S. M., and McCave, I. N.: Neogene overflow of Northern Component Water at the Greenland–Scotland Ridge, Geochem. Geophys. Geosyst., 7, Q06010, https://doi.org/10.1029/2005GC001085, 2006.

Ravelo, A. C., Andreasen, D. H., Lyle, M., Olivarez Lyle, A., and Wara, M. W.: Regional climate shifts caused by gradual global cooling in the Pliocene epoch, Nature, 429, 263–267, https://doi.org/10.1038/nature02567, 2004.

Raymo, M. E., Grant, B., Horowitz, M., and Rau, G. H.: Mid-Pliocene warmth: stronger greenhouse and stronger conveyor, Mar. Micropaleontol., 27 (1–4), 313–326, https://doi.org/10.1016/0377-8398(95)00048-8, 1996.

Rebesco, F., Hernández-Molina, J., Van Rooij, D., and Wåhlin, A.: Contourites and associated sediments controlled by deep-water circulation processes: State-of-the-art and future considerations, Marine Geol., 352, 111–154, https://doi.org/10.1016/j.margeo.2014.03.011, 2014.

Richardson, P. L.: On the history of meridional overturning circulation schematic diagrams, Prog. Oceanogr., 76 (4), 466–486, https://doi.org/10.1016/j.pocean.2008.01.005, 2008.

Roveri, M., Flecker, R., Krijgsman, W., Lofi, J., Lugli, S., Manzi, V., Sierro, F. J., Bertini, A., Camerlenghi, A., De Lange, G., Govers, R., Hilgen, F. J., Hübscher, C., Meijer, P. Th., and Stoica, M.: The Messinian Salinity Crisis: Past and future of a great challenge for marine sciences, Marine Geol., 352, 25–58. https://doi.org/10.1016/j.margeo.2014.02.002, 2014.

Roveri, M., Lugli, S., and Manzi, V.: The desiccation and catastrophic refilling of the Mediterranean: 50 years of facts, hypotheses, and myths around the Messinian Salinity Crisis, Annu. Rev. Mar. Sci., 17, 485–509, https://doi.org/10.1146/annurev-marine-021723-110155, 2025.

Shackleton, N. J., Hall, M. A., and Pate, D.: Pliocene Stable Isotope Stratigraphy of Site 846, edited by: Pisias, N. G., Mayer, L. A., Janecek, T. R., Palmer-Julson, A., and van Andel, T. H., Proc. ODP, Sci. Results, 138, 337–355, 1995.

Shaffer, G., and Bendtsen, J.: Role of the Bering Strait in controlling North Atlantic ocean circulation and climate, Nature, 367, 354–357, https://doi.org/10.1038/367354a0, 1994.

Sigman, D. M. and Boyle, E. A.: Glacial/interglacial variations in atmospheric carbon dioxide, Nature, 407, 859–869, https://doi.org/10.1038/35038000, 2000.

Sinnesael, M., Karatsolis, B.-T., Pearson, P. N., Briais, A., Hemming, S. R., LeVay, L. J., Dunkley Jones, T., Cui, Y., Di Chiara, A., Dodd, J. P., Dwyer, D., Eason, D. E., Friedman, S. A., Hanson, E., Hochmuth, K., Ibrahim, H. E., Jasper, C. E., Lee-Takeda, S., LeBlanc, D. E., Lindsay, M. R., McNamara, D. D., Modestou, S. E., Morris, M. A., Murton, B. J., OConnell, S., Pasquet, G., Qian, S.-P., Rosenthal, Y., Satolli, S., Suzuki, T., Thulasi, T., Wade, B. S., White, N. J., Wu, T., Yang, A. Y., and Parnell-Turner, R. E.: Onset of strong Iceland-Scotland overflow water 3.6 million years ago, Nat Commun., 16, 4323. https://doi.org/10.1038/s41467-025-59265-5, 2025.

Sniderman, J. M. K., Woodhead, J. D., Hellstrom, J., Jordan, G. J., Drysdale, R. N., Tyler, J. J., and Porch, N.: Pliocene reversal of late Neogene aridification, Proc. Natl. Acad. Sci. U.S.A., 113 (8), 1999–2004, https://doi.org/10.1073/pnas.1520188113, 2016.

Steinfeldt, R., Rhein, M., Bullister, J. L., and Tanhua, T.: Inventory changes in anthropogenic carbon from 1997–2003 in the Atlantic Ocean between 20°S and 65°N, Global Biogeochem. Cycles, 23, GB3010, https://doi.org/10.1029/2008GB003311, 2009.

Steinthorsdottir, M., Coxall, H. K., De Boer, A. M., Huber, M., Barbolini, N., Bradshaw, C. D., Burls, N. J., Feakins, S. J., Gasson, E., Henderiks, J., Holbourn, A. E., Kiel, S., Kohn, M. J., Knorr, G., Kürschner, W. M., Lear, C. H., Liebrand, D., Lunt, D. J., Mörs, T., Pearson, P. N., Pound, M. J., Stoll, H., and Strömberg, C. A. E.: The Miocene: The future of the past, Paleoceanog. Paleoclimatol., 36, e2020PA004037, https://doi.org/10.1029/2020PA004037, 2021.

Stocker, T. F., and Schmittner, A.: Influence of CO_2 emission rates on the stability of the thermohaline circulation, Nature, 388, 862–865, https://doi.org/10.1038/42224, 1997.

Takahashi, T., Sutherland, S. C., Wanninkhof, R., Sweeney, C., Feely, R. A., Chipman, D. W., Hales, B., Friederich, G., Chavez, F., Sabine, C., Watson, A., Bakker, D. C. E., Schuster, U., Metzl, N., Yoshikawa-Inoue, H., Ishii, M., Midorikawa, T., Nojiri, Y., Körtzinger, A., Steinhoff, T., Hoppema, M., Olafsson, J., Arnarson, T. S., Tilbrook, B., Johannessen, T., Olsen, A., Bellerby, R., Wong, C. S., Delille, B., Bates, N. R., and de Baar, H. J. W.: Climatological mean and decadal change in surface ocean pCO_2, and net sea–air CO_2 flux over the global oceans, Deep Sea Res. II, 56 (8–10), 554–577, https://doi.org/10.1016/j.dsr2.2008.12.009, 2009.

Tierney, J. E., Poulsen, C. J., Montañez, I. P., Bhattacharya, T., Feng, R., Ford, H. L., Hönisch, B., Inglis, G. N., Petersen, S. V., Sagoo, N., Tabor, C. R., Thirumalai, K., Zhu, J., Burls, N. J., Foster, G. L., Goddéris, Y., Huber, B. T., Ivany, L. C., Kirtland Turner, S., McElwain, J. C., Mills, B. J. W., Otto-Bliesner, B. L., Ridgwell, A., and Zhang, Y. G.: Past climates inform our future, Science, 370, eaay3701, https://doi.org/10.1126/science.aay3701, 2020.

Tindall, J. C., and Haywood, A. M.: Modelling the mid-Pliocene warm period using HadGEM2, Glob. Planet. Change, 186, 103110, https://doi.org/10.1016/j.gloplacha.2019.103110, 2019.

Toggweiler, J. R., Russell, J. L., and Carson, S. R.: Midlatitude westerlies, atmospheric CO_2, and climate change during the ice ages, Paleoceanography, 21, PA2005, https://doi.org/10.1029/2005PA001154, 2006.

Toucanne, S., Soulet, G., Riveiros, N. V., Boswell, S. M., Dennielou, B., Waelbroeck, C., Bayon, G., Mojtahid, M., Bosq, M., Sabine, M., Zaragosi, S., Bourillet, J.-F., and Mercier, H.: The North Atlantic glacial Eastern Boundary Current as a key driver for ice-sheet–AMOC interactions and climate instability, Paleoceanogr. Paleoclimatol., 36, e2020PA004068, https://doi.org/10.1029/2020PA004068, 2021.

Uitz, J., Claustre, H., Gentili, B., and Stramski, D.: Phytoplankton class-specific primary production in the world's oceans: Seasonal and interannual variability from satellite observations, Global Biogeochem. Cycles, 24, GB3016, https://doi.org/10.1029/2009GB003680, 2010.

https://doi.org/10.5194/egusphere-2026-3764
Preprint. Discussion started: 7 July 2026

Volk, T. and Hoffert, M. I.: Ocean Carbon Pumps: Analysis of Relative Strengths and Efficiencies in Ocean-Driven Atmospheric CO_2 Changes, in: The Carbon Cycle and Atmospheric CO_2: Natural Variations Archean to Present, edited by Sundquist, E. T. and Broecker, W. S., American Geophysical Union, Washington, D.C., 99–110, https://doi.org/10.1029/GM032p0099, 1985.

Wang, S.-J., Cao, L., and Li, N.: Responses of the ocean carbon cycle to climate change: results from an Earth system climate model simulation, Adv. Clim. Change Res., 5 (3), 123–130, https://doi.org/10.1016/j.accre.2014.11.004, 2014.

Wen, Y., Zhang, L., Holbourn, A. E., Zhu, C., Huntington, K. W., Jin, T., Li, Y., and Wang, C.: CO_2-forced late Miocene cooling and ecosystem reorganizations in East Asia, Proc. Natl. Acad. Sci. U.S.A., 120 (5), e2214655120, https://doi.org/10.1073/pnas.2214655120, 2023.

Wold, C. N.: Cenozoic sediment accumulation on drifts in the northern North Atlantic, Paleoceanography, 9, 917–941, 1994.

Wright, J. D., and K. G. Miller: Control of North Atlantic Deep Water Circulation by the Greenland-Scotland Ridge, Paleoceanography, 11 (2), 157–170, https://doi.org/10.1029/95PA03696, 1996.

Wu, L., Wilson, D. J., Wang, R., Yin, X., Chen, Z., Xiao, W., and Huang, M.: Evaluating Zr/Rb ratio from XRF scanning as an indicator of grain-size variations of glaciomarine sediments in the Southern Ocean, Geochem. Geophys. Geosyst., 21, e2020GC009350, https://doi.org/10.1029/2020GC009350, 2020.